Radiating Instabilities of Thin Baroclinic Jets

L. D. TALLEY

School of Oceanography, Oregon State University, Corvallis, OR 97331

(Manuscript received 14 January 1983, in final form 4 August 1983)

ABSTRACT

The linear stability of thin, quasi-geostrophic, two-layer zonal jets on the β-plane is considered. The meridional structure of the jets is approximated in such a way as to allow an exact dispersion relation to be found. Necessary conditions for instability and energy integrals are extended to these piece-wise continuous profiles. The linearly unstable modes which arise can be related directly to instabilities arising from the vertical and horizontal shear. It is found empirically that the necessary conditions for instability are sufficient for the cases considered. Attention is focused on unstable modes that penetrate far into the locally stable ocean interior and which are found when conditions allow the jet instability phase speeds to overlap the far-field, free-wave phase speeds. These radiating instabilities exist in addition to more unstable waves which are trapped within a few deformation radii of the jet. The growth rates of the radiating instabilities depend strongly on the size of the overlap of instability and free-wave phase speeds. The extreme cases of this are westward jets which have vigorously growing, radiating instabilities and purely eastward jets which do not radiate at all. Radiating instabilities are divided into two types: a subset of the jets' main unstable waves near marginal stability and instabilities which appear to be destabilized free waves of the interior ocean. It is suggested that the fully developed field of instabilities of a zonal current consists of the most unstable, trapped waves directly in the current with a shift to less unstable, radiating waves some distance from the current. A brief comparison of the model results with observations south of the Gulf Stream is made.

1. Introduction

In many parts of the ocean, the circulation is concentrated in narrow currents. These currents are nearly zonal and may be modeled as quasi-geostrophic jets. The jets are usually baroclinic as well as having large horizontal shear. Thus they may have the capacity for both baroclinic and barotropic instability. Ocean observations show that variability in velocity and density is very large in and near such currents (e.g. Dantzler, 1977; Richardson, 1983; Schmitz, 1978; Bernstein and White, 1977; Schmitz *et al.*, 1982). The variability is undoubtedly due to instability [see Philander (1978) for a review of eddy energy-producing mechanisms]. The energy from the instabilities of these intense currents finds its way into the gyre interiors: one mechanism which is being explored is the propagation and decay of Gulf Stream rings (Flierl, 1977; Flierl *et al.*, 1980). It is the purpose of this paper to explore a related possibility: namely, that the structure of the eddy field south of the Gulf Stream can be understood through a consideration of the unstable modes of the Gulf Stream itself.

In this paper the linearly unstable modes of symmetric, quasi-geostrophic jets which have both horizontal and vertical shear are determined. All unstable jets have instabilities which are trapped to the jet, penetrating only a short distance into the stable (or less unstable) bordering regions. Another type of instability which penetrates large distances into bordering regions is "radiating", as explored by Dickinson and Clare (1973) in the context of parallel shear flow. A major focus of this paper is the existence and structure of these radiating instabilities, which take the form of modified Rossby waves in the ocean interior. A condition for the existence of radiating instabilities is that the phase speeds and x-wavenumbers of the jet instabilities and the modified Rossby waves correspond. This condition predisposes westward, barotropic jets to radiate while eastward, barotropic jets do not radiate (Talley, 1983). The same is true of simple westward and eastward baroclinic jets, as seen in this paper. If eastward, barotropic jets are modified slightly, by introducing vertical shear in the far-field or vertical undercurrent, radiating instabilities can be produced. When radiation is possible, in that the instability phase speeds and Rossby wave phase speeds overlap, large numbers of radiating instabilities are found in addition to trapped modes.

Previous investigators (e.g., McIntyre and Weissman, 1978; Dickinson and Clare, 1973) have suggested that the linear growth rates of radiating instabilities are much lower than those of trapped instabilities. It is found here that, while radiating instabilities do have lower growth rates than the most unstable, trapped instabilities, in some cases their growth rates can be nearly as large as those of the most unstable waves, for instance for a westward jet. In addition, for some parameter ranges, all instabilities are radiating.

The present paper is concerned with linear insta-

bilities which radiate. It is apparent from studies of nonlinear stability of vertically sheared flows that are unstable to Kelvin–Helmholtz modes and that also can support internal gravity waves that linearly radiating instabilities can be produced (Lindzen and Rosenthal, 1976), that the nonlinear evolution of trapped instabilities might result in radiation (Edmon, *et al.*, 1980) and that trapped Kelvin–Helmholtz instabilities can interact nonlinearly to produce a radiating internal gravity wave (Fritts, 1982). Nonlinear mechanisms for production of radiating quasi-geostrophic waves are not explored in this paper: the two cited cases of nonlinear production of radiating waves would presumably carry over to the quasi-geostrophic problem.

There have been several thorough parameter studies of mixed baroclinic–barotropic instability using a two-layer model. Orlanski (1969) considered the effects of topography and varying stratification on the stability of a baroclinic jet. Hart (1974) showed how the relative importance of barotropic and baroclinic instability depends on the relative layer depths and Froude number. Gent (1974, 1975) discussed the effect of variable jet widths and β on the unstable modes, showing that the meridional scale of the most unstable wave is set by the jet width rather than the Rossby deformation radius. Haidvogel and Holland (1978) showed that a linear stability analysis of instantaneous and time-averaged flow profiles taken from two-layer, eddy-resolving general circulation models yields meaningful results for the lowest order properties (wavenumber, phase speed and growth rate) of the dominant waves in the complete model. The higher order quantities (Reynolds stress and heat flux) were not predicted as well by the linear stability analysis. They also found that proper simulation of the barotropic instability process requires a velocity profile that is closer to the instantaneous velocity than to the time-averaged flow since the sharpness of the Gulf Stream is lost in averaging because of meandering. Holland and Haidvogel (1980) investigated the effect of changes in the amount of horizontal shear in the lower layer, Froude number, relative layer depths and ratio of β to the relative vorticity on the relative importance of barotropic and baroclinic instability. The jet that they considered is similar to one of the cases considered here. Their dispersion relations were similar to those here and must therefore have included radiating instabilities. However, their focus was on the most unstable waves, which were trapped, so the radiating nature of some of the instabilities was not made clear.

Pedlosky (1977) showed how modified, neutral Rossby waves in a vertically sheared flow could be forced by a corrugated, vertical, moving boundary. The flow was stable because of large, non-zero β. The forced waves were either evanescent or radiating depending on whether the phase speed condition was satisfied. The present study extends this idea to the motivating situation, namely that periodic instabilities of a zonal current might excite the ambient waves of the far field which then transmit energy from the current far into the ocean interior.

It is hypothesized here that the fully nonlinear flow contains more than just the initial basic flow and the most unstable wave: it is suggested that waves with lower growth rates survive and grow and that these waves, which have much larger meridional decay scales than the more unstable waves, dominate the far field of the jet while the most unstable waves are most important right in the jet.

The chief importance in the present results, in addition to being yet another discussion of the linearly unstable modes of zonal flows, is that they suggest that at least part of the mid-ocean eddy field can be generated some distance away by more intense currents. The results only suggest this possibility since we cannot predict from linear stability analysis alone which instabilities will survive to dominate the fully nonlinear flow.

The model is defined in Section 2: all flows are symmetric, two-layer jets with strong horizontal and vertical shear. The jets are simplified using an extension of Rayleigh's (1879) method to two-layer flow on the β-plane. In Section 3 linear stability results are given for nonradiating and radiating jets. Two types of radiating instability are found: 1) trapped instabilities of a nonradiating jet which are enabled to radiate by a slight change in the jet profile and 2) destabilized Rossby waves of the far field. In Section 4, a qualitative comparison of the model and the eddy field near the Gulf Stream is made.

2. The basic problem

The stability of narrow, intense baroclinic jets is examined here using two simplifications for the flow profiles: the vertical structure is represented by a two-layer model in which the two layers have equal depth, thus retaining only two vertical modes; the horizontal shear is restricted to specific zones, using flow profiles similar to Rayleigh's (1879) "broken line" profiles. It is assumed that the basic flow is zonal and steady and that the perturbation streamfunction has much smaller amplitude than the mean flow streamfunction. The quasi-geostrophic, linearized, inviscid, nondimensional potential vorticity equations for the perturbations in the two layers are (cf. Pedlosky, 1979):

$$\left(\frac{\partial}{\partial t} + U_n \frac{\partial}{\partial x}\right)[\nabla_H^2 \phi_n - (-1)^n F(\phi_2 - \phi_1)] + \frac{\partial Q_n}{\partial y}\frac{\partial \phi_n}{\partial x} = 0, \quad n = 1, 2. \quad (1)$$

Here, (∇_H^2) is the two-dimensional Laplacian $(\partial^2/\partial x^2 + \partial^2/\partial y^2)$, and ϕ_1 and ϕ_2 are the perturbation streamfunctions for the top and bottom layers, respectively. The equations were scaled using L, U and H (horizontal

length, flow velocity and layer depth). The non-dimensional parameters are $\beta = \beta_0 L^2/U$ and $F = (L/L_R)^2$ where L_R is the internal deformation radius, $L_R = (g'/f)^{1/2}$. The mean flow, U_1 and U_2, depends only on latitude y. The potential vorticity gradient for the mean flow in each layer and in each horizontal region is

$$\frac{\partial Q_n}{\partial y} = \beta - U_{nyy} - (-1)^n F(U_1 - U_2), \quad n = 1, 2.$$

The boundary conditions are that the disturbances ϕ_1 and ϕ_2 be bounded at $y = \pm\infty$ if the ocean is unbounded. If the wave is not growing and is purely oscillatory in y, the boundary condition at $y = \pm\infty$ is that the meridional group velocity be outward. If there are zonal boundaries at $y = \pm H$, $\phi_1 = \phi_2 = 0$ at the boundaries.

Normal mode solutions to (1) are sought, with $\phi_1 = \Phi_1(y)e^{ik(x-ct)}$ and $\phi_2 = \Phi_2(y)e^{ik(x-ct)}$. Both c and Φ_n are allowed to be complex while k is strictly real. Eq. (1) becomes

$$(U_n - c)\left\{\frac{d^2\Phi_n}{dy^2} - k^2\Phi_n - (-1)^n F(\Phi_2 - \Phi_1)\right\} + \frac{\partial Q_n}{\partial y}\Phi_n = 0, \quad n = 1, 2. \quad (2)$$

Specific flows are modeled by piecing together regions in which either

$$U_1, U_2 = \text{constants} \quad (3a)$$

or

$$\frac{\partial Q_1}{\partial y} = \frac{\partial Q_2}{\partial y} = 0 \quad (3b)$$

so that, in a given region, either the flow speeds are constant or the potential vorticity gradient vanishes. The flow is illustrated in Fig. 1. The length scale used in non-dimensionalization is the half-width of the central jet (Region I). The shear zone (Region II) is $1 < |y| < D$. Boundaries are at $|y| = H$ where $H \gg L$ (in most models considered here, $H \to \infty$). The velocity is specified in the upper and lower layers in the central jet (U_{I1}, U_{I2}) and outside the jet (U_{01}, U_{02}). Velocity is scaled by U_{I1}^*. Also, $U_{02} = 0$ in all models.

Because the horizontal velocity gradient dU_n/dy has discontinuities, the overall potential vorticity gradient, including the points of discontinuity, will have delta function contributions. The necessary conditions for instability in two-layer flows (Pedlosky, 1979) are of course influenced by these delta functions. As given by Talley (1983), the effective potential vorticity gradient, which includes these delta function contributions, is

$$\frac{\partial \hat{Q}_n}{\partial y} = \frac{\partial Q_n}{\partial y} - \left[\frac{dU_n}{dy}\right]_{y_0}\delta(y - y_0), \quad (4)$$

where brackets indicates the jump in the quantity at

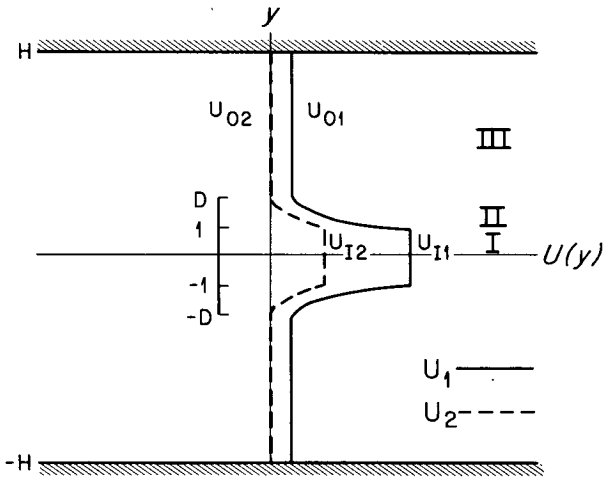

FIG. 1. Baroclinic jet modeled with two layers and meridional regions of uniform velocity or uniform potential vorticity. In most cases examined, there are no boundaries at $|y| = H$.

$y = y_0$. The necessary conditions for instability can be written as

$$c_i \sum_{n=1}^{2} \int_{-H}^{H} dy \frac{|\Phi_n|}{|U_n - c|^2} \frac{\partial \hat{Q}_n}{\partial y} = 0, \quad (5a)$$

$$\sum_{n=1}^{2} \int_{-H}^{H} dy \frac{|\Phi_n|^2}{|U_n - c|^2}(U_n - c_r)\frac{\partial \hat{Q}_n}{\partial y} > 0. \quad (5b)$$

In evaluating the necessary conditions for instability, the delta function contributions must be taken into account: indeed in the purely barotropic analog of the present model, the delta functions are the *only* nonzero contributions to the potential vorticity gradient.

It is necessary to examine the energy integral to determine whether discontinuities in U_n or dU_n/dy change the usual expressions for transfer from mean kinetic energy to the perturbation kinetic energy (Pedlosky, 1979). Details of the derivation of the energy equation are given in the Appendix. When the kinetic energy transfer terms are written in the form $(-\overline{u_n'v_n'})dU_n/dy$ and U_n is continuous, there are no changes in the energy equation, because dU_n/dy is simply discontinuous. The energy transfer equation is

$$\int_{-H}^{H} \frac{\partial \overline{E(\phi)}}{\partial t} dy = \int_{-H}^{H} \left[\overline{\phi_{1x}\phi_{1y}}\frac{dU_1}{dy} + \overline{\phi_{2x}\phi_{2y}}\frac{dU_2}{dy} + F(U_1 - U_2)\overline{\phi_1\phi_{2x}}\right] dy, \quad (6)$$

where

$$\overline{E(\phi)} = \frac{F}{2}\overline{(\phi_1 - \phi_2)^2} + \sum_{n=1}^{2}\frac{1}{2}[\overline{(\phi_{nx})^2} + \overline{(\phi_{ny})^2}].$$

These terms will be used to determine the relative importance of kinetic and potential energy transfers.

The kinetic energy terms, of course, are non-zero only in Region II, where dU_n/dy is non-zero.

Limits on the complex phase speed of instabilities are given by Howard (1961) and Pedlosky (1964). Radiating instability might occur when the range of instability phase speeds overlaps the range of phase speeds of modified Rossby waves in the irradiated region (McIntyre and Weissman, 1978). Thus the possibility of radiation is easily predicted in advance of actual examination of a flow's instability. Radiating instabilities are defined by Talley (1983). In short, they are instabilities that are adjacent to neutral modes that have purely real y-wavenumbers in the irradiated region. The neutral modes are Rossby waves, modified if there is vertical shear. The radiating instabilities investigated here do not depend on the presence of boundaries at $|y| = H$: with the exception of a discussion of the effect of zonal boundaries on the radiating instabilities at the end of Section 3, all models considered have no zonal boundaries. Previous discussions point out the possibility of two types of radiating instability: those which depend on the presence of boundaries and those which arise solely from the jet. The present investigator did not discover any instabilities which were solely due to the presence of zonal boundaries, but the investigation of these cases was admittedly less thorough.

Solutions to the potential vorticity equation (2) are found for Regions I, II and III subject to boundary conditions at $y = \pm H$ or $\pm\infty$ and to matching conditions at the breaks between the regions. Matching conditions are obtained by requiring that there be no delta function contributions to the continuity and potential vorticity equations at the breaks. When the continuity equation is integrated across a profile break, we obtain the condition

$$\left[\frac{\partial \eta_n}{\partial t}\right]_{y_0} = 0, \quad n = 1, 2,$$

where η_n is the interface displacement, $v_n = D\eta_n/Dt$, and square brackets indicate a jump in the quantity at y_0. In normal mode form, this becomes

$$\left[\frac{\Phi_n}{U_n - c}\right]_{y_0} = 0. \tag{7a}$$

This condition is equivalent to requiring that the normal velocity and interface displacement be continuous. When the potential vorticity equation is integrated across a break, we obtain

$$\left[\frac{Du_n}{Dt}\right]_{y_0} = 0, \quad n = 1, 2.$$

In normal mode form, this becomes

$$\left[(U_n - c)\frac{d\Phi_n}{dy} - \Phi_n \frac{dU_n}{dy}\right]_{y_0} = 0. \tag{7b}$$

The matching conditions (7a, b) are identical to those used in the barotropic instability problem.

In order to solve (2), we must first solve (3b) for U_1 and U_2 in Region II, requiring that they be continuous at $y = 1$ and D. The flow profile is thus

$$U_1(y) = \frac{\beta^2}{2} + c_1 + c_2 y + c_3 \cosh(2F)^{1/2} y + c_4 \sinh(2F)^{1/2} y, \tag{8a}$$

$$U_2(y) = \frac{\beta^2}{2} + c_1 + c_2 y - c_3 \cosh(2F)^{1/2} y - c_4 \sinh(2F)^{1/2} y, \tag{8b}$$

where

$$c_1 = \frac{(U_{11} + U_{12})D - (U_{01} + U_{02})}{2(D-1)} + \frac{\beta D}{2},$$

$$c_2 = \frac{(U_{01} + U_{02})D - (U_{11} + U_{12})}{2(D-1)} - \frac{\beta(D-1)}{2},$$

$$c_3 = \frac{(U_{01} - U_{02})\sinh(2F)^{1/2} + (U_{11} - U_{12})\sinh(2F)^{1/2} D}{2\sinh(2F)^{1/2}(D-1)},$$

$$c_4 = \frac{(U_{01} - U_{02})\cosh(2F)^{1/2} - (U_{11} - U_{12})\cosh(2F)^{1/2} D}{2\sinh(2F)^{1/2}(D-1)}.$$

Note that if the velocity in, say, the lower layer is the same in Regions I and III ($U_{1n} = U_{0n}$), there is still horizontal shear in Region II since the potential vorticity gradient is required to vanish there.

In Regions I and III, $\partial Q_n/\partial y = \beta - (-1)^n F(U_1 - U_2)$, independent of y. Seeking solutions to (3) of the form $\Phi_n = A_n e^{ry}$, we find:

$$\frac{A_2}{A_1} = -\frac{(U_1 - c)(r^2 - k^2 - F) + \beta + F(U_1 - U_2)}{F(U_1 - c)}, \tag{9}$$

where

$$r_\pm^2 = k^2 - \frac{\beta(U_1 + U_2 - 2c)}{2(U_1 - c)(U_2 - c)} + F + \frac{F(U_1 - U_2)^2}{2(U_1 - c)(U_2 - c)} \pm \frac{1}{2(U_1 - c)(U_2 - c)} \{\beta^2 (U_1 - U_2)^2 - 2\beta F(U_1 + U_2 - 2c)(U_1 - U_2)^2 + F^2[(U_1 - U_2)^2 + 2(U_1 - c)(U_2 - c)]^2\}^{1/2}. \tag{10}$$

In Region II where the potential vorticity gradient is zero,

$$\left.\begin{aligned} r_+^2 &= k^2 + 2F \\ r_-^2 &= k^2. \end{aligned}\right\}$$

The associated amplitude ratios (9) are -1 and 1, re-

spectively. These are the baroclinic and barotropic modes and are also the correct solutions in regions I and III when β and (U_1 and U_2) are zero.

Only symmetric solutions are sought. The antisymmetric (varicose) solutions were discarded because their growth rates are generally lower than those of the sinuous mode in the barotropic problem (Talley, 1983). In the jet itself, the most unstable wave will probably dominate, so it may be justified to omit the varicose mode for the near field. However, it is argued in this paper that weakly growing, radiating waves may be important in the far field (Region III), so elimination of the varicose modes may not be altogether justified.

The symmetric solution Φ_n in regions I, II and III is

$$\text{I)}\quad \left.\begin{aligned}\Phi_1 &= a_1e^{my} + a_2e^{-my} + a_3e^{\hat{m}y} + a_4e^{-\hat{m}y}\\ \Phi_2 &= f(a_1e^{my} + a_2e^{-my}) + \hat{f}(a_3e^{\hat{m}y} + a_4e^{-\hat{m}y})\end{aligned}\right\}. \tag{11a}$$

$$\text{II)}\quad \left.\begin{aligned}\Phi_1 &= b_1e^{ky} + b_2e^{-ky} + b_3e^{ly} + b_4e^{-ly}\\ \Phi_2 &= b_1e^{ky} + b_2e^{-ky} - b_3e^{ly} - b_4e^{-ly}\end{aligned}\right\}, \tag{11b}$$

$$\text{III)}\quad \left.\begin{aligned}\Phi_1 &= d_1e^{py} + d_2e^{-py} + d_3e^{\hat{p}y} + d_4e^{-\hat{p}y}\\ \Phi_2 &= g(d_1e^{py} + d_2e^{-py}) + \hat{g}(d_3e^{\hat{p}y} + d_4e^{-\hat{p}y})\end{aligned}\right\}. \tag{11c}$$

Here m, $\hat{m}$, f and $\hat{f}$ correspond to r_-, r_+ and the associated A_2/A_1 in (9) and (8) with $U_n = U_{1n}$; p, $\hat{p}$, g and $\hat{g}$ correspond to r_-, r_+ and the associated A_2/A_1 with $U_n = U_{0n}$; $l = (k^2 + 2F)^{1/2}$. Application of the boundary conditions and matching conditions then allows evaluation of all but one of the coefficients a_n, b_n and d_n and yields the dispersion relation, $c(k)$. The transcendental equation for c is solved numerically using the secant method with complex arithmetic.

Instability is possible when the necessary conditions for instability (5) are satisfied. One requirement is that the potential vorticity gradient change sign (5a). This may occur if $\beta + F(U_1 - U_2)$ and $\beta - (U_1 - U_2)$ are of opposite sign in either Region I or III: since this is the usual necessary condition for *baroclinic* instability, unstable modes which result from this condition being satisfied may be referred to as *vertical shear* modes, even if the flow is simultaneously barotropically unstable.

The effective potential vorticity gradient may also change sign if the portion equivalent to $\beta - U_{nyy}$ changes sign. The only non-zero contributions to U_{nyy} which affect the conditions (5) are delta functions at the profile breaks, so satisfaction of this condition requires that the delta function be negative which in turn requires that dU_n/dy be of the proper sign (4). Modes which arise when $\beta - U_{nyy}$ changes sign may be referred to as *horizontal shear* modes, even if the flow is also baroclinically unstable.

A third possibility for sign change of $\partial\hat{Q}_n/\partial y$ is when $\beta \pm F(U_1 - U_2)$ changes sign from Region I to Region III. Since this relies on there being both horizontal and vertical shear, instabilities that arise because of this change may be called *mixed*. However, the second necessary condition for instability (5b) eliminates these instabilities when there is no net horizontal shear in the lower layer (when $U_{12} = U_{02}$), which is the geometry of most examples explored in the following section.

The usual definition of mixed instabilities is that they draw energy from both the mean kinetic and potential energy. For jets considered here, all modes of instability are mixed in this sense for some portion of the parameter ranges. I have, however, chosen to identify the modes of instability by the ranges of parameters for which they occur and by their presence or absence when either the horizontal or vertical shear is removed. Thus, a horizontal shear mode will disappear when the horizontal shear is removed, etc. A mixed instability will disappear when either the horizontal or vertical shear is removed. In actuality, for the profiles considered in this paper, the definition of mixed instabilities could not be tested since no mixed instabilities were possible, because of the necessary condition for instability (5b).

3. Results

The stability of the simple flows described in this paper depends on a large number of parameters: the relative vertical shear in and outside the jet, the relative width of the horizontal shear zones, the internal deformation radius, the total width of the zonal channel, β and the zonal wavenumber k. In all examples that follow, the shape of the jet, the deformation radius and the width of the channel are set and then β and k are varied.

The stability of flows with a jet in the upper layer and (nearly) no flow in the lower layer is considered first. The flow is thus similar to the barotropic jet considered by Talley (1983) with the addition of a vertical shear in the jet and thus an additional energy source. The energetics and structure of the unstable modes are strongly affected by the addition of vertical shear, so this flow is treated in some detail here. Just as for the barotropic jet, the basic, eastward, baroclinic jet has no radiating solutions while a westward baroclinic jet radiates vigorously. In order for a basically eastward jet to radiate, the flow in the outer regions or the lower layer must be modified somewhat so that the phase speed condition can be met. Three examples of such modified jets and their instabilities (non-radiating and radiating) are described. Finally, the effect of varying some of the flow parameters is explored.

a. *Basic jet*

The basic jet is illustrated in Fig. 2a. The profile is

$$\left.\begin{aligned}U_{11} = 1, \quad U_{12} = 0, \quad U_{02} = 0\\ F = 5, \quad D = 1.7, \quad H \to \infty\end{aligned}\right\}. \tag{12}$$

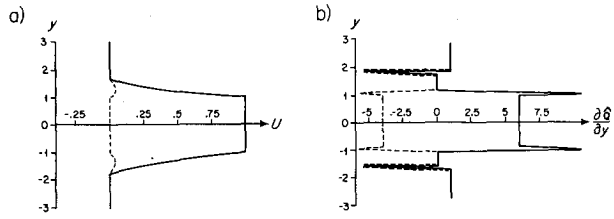

FIG. 2. (a) Velocity profile and (b) effective potential vorticity gradient at $\beta = 1$ for the basic jet (18). Solid curves are for the upper layer and dashed curves are for the lower layer. The spikes in (b) represent delta functions in $\partial \bar{Q}_n/\partial y$.

The basic jet has vertical shear in the central jet and horizontal shear in the upper layer. There is also a small amount of horizontal shear in the lower layer in the jet wings, on account of the constraint of zero potential-vorticity gradient.

The modes of instability that are possible for different parameter settings can be determined by using the necessary conditions for instability (4). The only parameter that is free after setting the profile (12) is β: the discussion following (11) outlines the way in which bounds on β for various types of instabilities are determined. Instability due to vertical shear in the central jet might be possible when $|\beta| < 5$. Instability due to horizontal shear in the upper layer might be possible when $-6.67 < \beta < 3.05$. There is no β for which the lower layer is barotropically unstable (i.e., for which the lower layer potential vorticity gradient satisfies the necessary conditions by itself) and also no β for which mixed instability, as defined in the previous section, can occur.

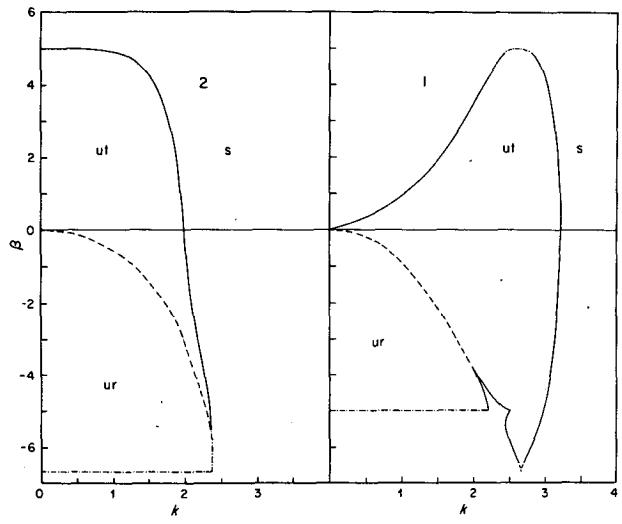

FIG. 3. Stability diagram in the β–k plane for the basic jet; "ut" are unstable, trapped waves, "ur" are unstable, radiating waves and "s" are stable waves. Solid curves are marginal stability curves, $c_i = 0$. Dot-dash curves are extrapolated marginal stability curves. Dashed curves are essentially the boundaries between trapped and radiating stabilities and are defined by $\mathrm{Im}(p) = \mathrm{Re}(p)$ where p is defined after (11c).

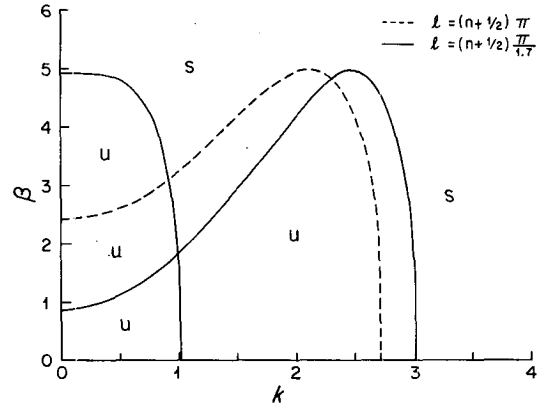

FIG. 4. Marginal stability curves for the two-layer model of baroclinic instability, where the layers have equal depths and the channel has half-width h (cf., Pedlosky, 1979). F is assumed to be 5 and $(U_1 - U_2) = 1.0$. β and k are varied. Two half-widths are used: $h = 1$ (dashed) and $h = 1.7$ (solid). There is one mode when $h = 1$ and two modes when $h = 1.7$.

The solution (11) and complex phase speed $c(k)$ were found for all values of β and k for which the flow is unstable. Fig. 3 shows the unstable region of the β–k plane. There are two modes of instability that basically correspond to the two lowest, cross-jet, baroclinically-unstable modes. The mode labeled "1" is the gravest and "2" the second cross-jet mode. (If the jet were a channel with rigid walls and half-width 1.7,

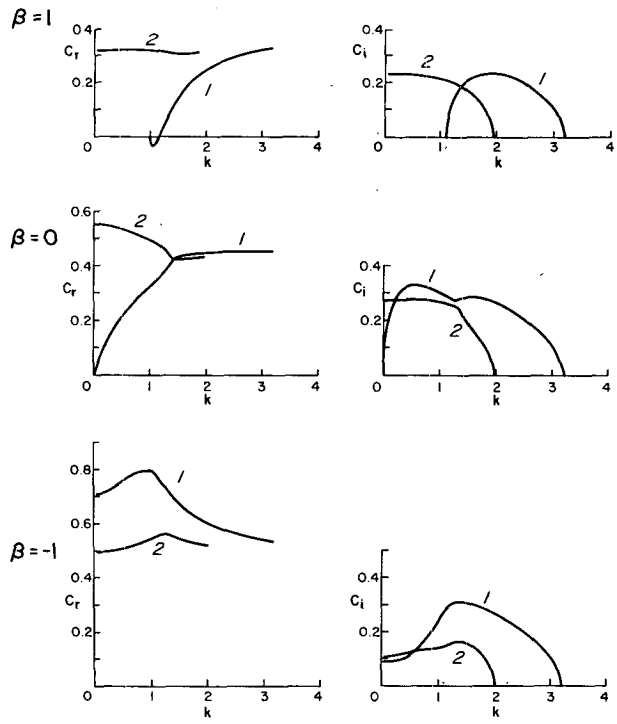

FIG. 5. The real and imaginary parts of the phase speed (c_r, c_i) as a function of zonal wavenumber for the basic jet instabilities at $\beta = 1$, 0 and -1.

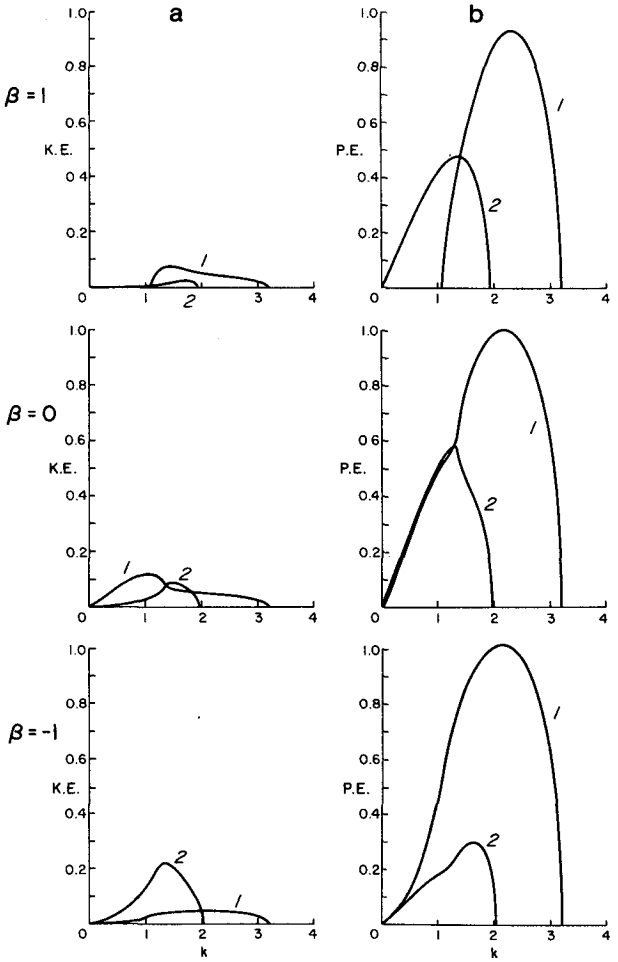

FIG. 6. (a) Transfer of kinetic energy to the instabilities from the upper-layer mean flow (U) and lower-layer mean flow (L) and (b) transfer of mean-flow potential energy, for the two modes of Fig. 3 (basic jet), at $\beta = 1$, 0 and -1.

it would have the modes of instability shown in Fig. 4: these clearly correspond well with the two modes of Fig. 3, for positive β.) For negative β, there is a dashed curve where the real and imaginary parts of p are equal: the significance of this curve is discussed below.

The complex phase speeds, energy transfers and complex meridional wavenumbers are shown in Figs. 5, 6 and 7. The most unstable eigenfunction at $\beta = 0$ for each of the two modes is shown in Fig. 8.

For positive β, all eigenfunctions are trapped: this can be seen from the complex meridional wavenumbers in Fig. 7 and from Fig. 8 which shows eigenfunctions that are typical of all positive-β eigenfunctions. From the necessary conditions for instability, we might have expected a horizontal shear mode for $\beta < 3.05$ in addition to the two modes that actually occur. In fact Mode 1 is a combination of horizontal and vertical shear modes: the energy transfers (Fig. 6) show a heightened kinetic energy source for the long waves of Mode 1. In Section 3c, we will see that the horizontal shear mode becomes a separate mode as the vertical shear is reduced and barotropic instabilities become more important.

When β is negative (westward jet), there are both trapped and radiating eigenfunctions. The dashed curve of Fig. 4 separates these two types. The long waves of both modes are radiating: they have weak meridional trapping and large meridional wavenumbers as can be seen in Fig. 7 for $\beta = -1$. A relatively large value of the imaginary part of p indicates that the free barotropic Rossby wave in the far field is being forced [discussion following (11c)]. Thus radiation in the form of barotropic Rossby waves occurs for both Modes 1 and 2 for small k.

The growth rates of the radiating waves are comparable to those of the trapped waves (Fig. 5) when β is negative. The radiating waves of Mode 1 are unstable to $\beta = -5$ and are thus associated with vertical shear instability (from the necessary conditions for instability) while the radiating waves of Mode 2 are unstable

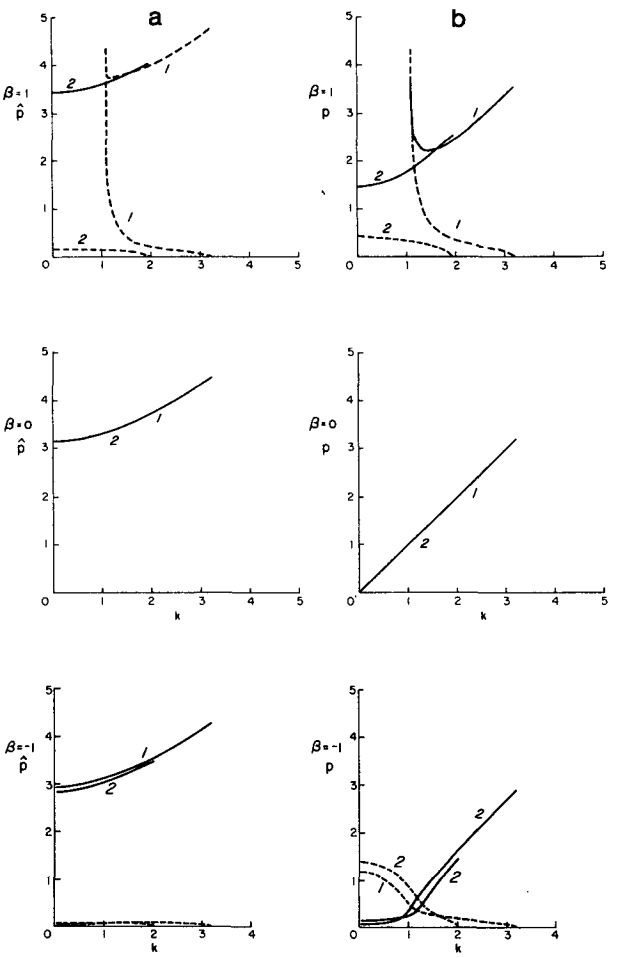

FIG. 7. Meridional dependence in Region III, the far field, of the basic jet at $\beta = -1$: (a) p and (b) $\hat{p}$, as defined in (11).

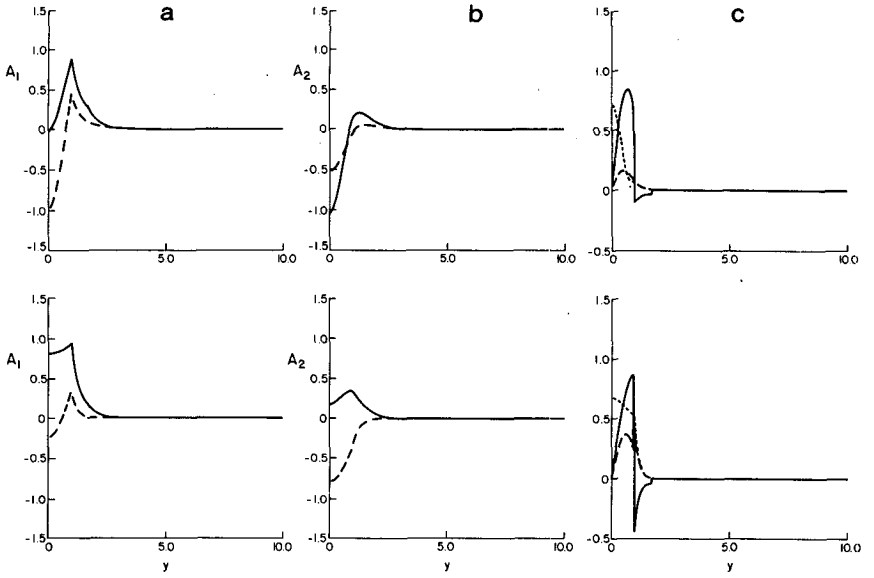

FIG. 8. Complex amplitudes of the most unstable eigenfunctions of Modes 2 (upper figures) and 1 (lower figures) at $\beta = 0$. (a) Real (solid) and imaginary (dashed) parts of the upper-layer amplitude A_1 and (b) lower-layer amplitude A_2. (c) Upper-layer momentum flux $\overline{u'v'}$ (solid), lower-layer momentum flux (long dash), heat flux $\overline{\phi_1\phi_{2x}}$ (short dash).

to $\beta = -6.67$ and are thus associated with horizontal shear instability. The trapped portion of Mode 1 is a combination of vertical and horizontal shear instabilities: note the contortions in the stability diagram at $\beta = -5$. Energy transfers (Fig. 6) are dominated by the baroclinic instability mechanism for $-5 < \beta < 0$. For $-6.67 < \beta < -5$, the necessary conditions for baroclinic instability are not satisfied but those for barotropic instability are: the energy source here is the mean-flow kinetic energy.

The radiating eigenfunctions are basically barotropic in the far field (Fig. 9) because only the barotropic Rossby wave in the far field is excited by the instability, regardless of whether the instabilities are fed by mean kinetic or potential energy. In Fig. 10, the phase speeds of the far-field baroclinic and barotropic Rossby waves are shown as a function of k for $l = 0$ and ∞. The instability phase speeds from Fig. 5 are replotted to show that the phase speed and wavenumber match only the barotropic Rossby wave.

For both positive and negative β, the basic jet is dominated by baroclinic instability: it has two unstable modes, both of which are basically vertical shear modes. The expected horizontal shear mode is merged with one of the vertical shear modes, affecting mainly its long wave behavior. The eastward jet does not radiate: although slightly negative phase speeds are possible with non-zero β (Pedlosky, 1979) from the semi-circle theorem, and although instabilities were found with slightly negative phase speeds (Fig. 5), none of the instabilities was radiating by any of the radiation criteria. This could not be predicted in advance. Tung (1981) showed that for barotropic instability the phase speeds of all marginally stable waves must be greater than $U_{\min}$ even if some instability phase speeds are negative: if this result carried over to the present case, it would rule out any radiating waves. However, Tung's result does not hold for two-layer baroclinic instability (Pedlosky, 1964) or for Green's model (Garcia and Norscini, 1970). There is thus no way confidently to

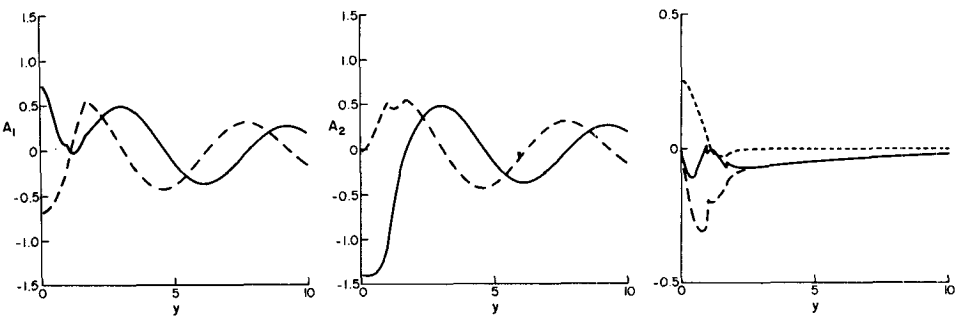

FIG. 9. Complex amplitude of radiating eigenfunction of the basic jet at $\beta = -1$, as in Fig. 8.

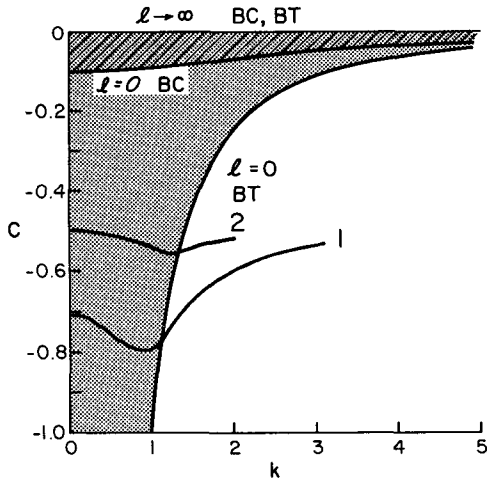

FIG. 10. Barotropic and baroclinic Rossby wave dispersion relations at $\beta = 1$ for $l = 0$ and $l \to \infty$. The shaded regions indicate where all Rossby waves lie. Superimposed on the diagram is c_r of the westward basic jet ($\beta = -1$) from Fig. 5.

predict a lack of radiating instabilities for the eastward, baroclinic jet, although they seem rather unlikely.

The westward jet has vigorously radiating modes in addition to trapped instabilities. One set of radiating waves (Mode 1) is associated with the horizontal shear while the other is associated with the vertical shear, according to their β-cutoffs and the necessary conditions for instability for identification.

b. Eastward, radiating jets

The eastward jet described in the previous section had no radiating solutions because the wavenumber and phase speed of its instabilities were unable to match the wavenumber and phase speed of ambient Rossby waves in the far field. The westward jet, on the other hand, had a wide range of radiating instabilities, with growth rates nearly comparable to the growth rates of the trapped waves. This is important in itself because it indicates that westward currents are more susceptible to radiation than eastward currents. Predominantly eastward jets can also radiate if slightly modified. The two simplest changes are to allow vertical shear in the far field and to include westward flow beneath the jet, in the lower layer. Both modifications result in greater overlap of instability and far-field Rossby-wave phase speeds. The results of such modifications are discussed briefly in this section. A more complicated change would be to allow westward flow in side lobes north and south of the main eastward jet—such a flow may be more realistic as far as the Gulf Stream or Kuroshio are concerned.

The three modified eastward jets are shown in Fig. 11. In addition to the types of instability which were possible for the basic jet, there can also be baroclinic instability in the far field when there is vertical shear there. The baroclinic instability modes have rather low growth rates and are stabilized by much lower values of β than the jet instabilities. It is conceivable that they might be important in radiation of jet instabilities at low β; however, empirically it was found that they are not involved in radiation of the jets considered and that only neutral waves of the far field match to jet instabilities. Apparently the additional constraint of matching c_i in addition to k and c_r is too strong.

1) EASTWARD JET WITH POSITIVE VERTICAL SHEAR IN THE FAR FIELD

We look first at the profile with weak, positive vertical shear in the far field (Fig. 11a). The flow is identical to (12) and Fig. 2, except that $U_{01} = 0.15$. Only positive β is considered. The necessary conditions for instability of the jets' vertical shear are unchanged: instability might be possible when $\beta < 5$. Because the horizontal shear of the upper layer is somewhat reduced, instability in the upper layer might occur only when $\beta < 2.05$. Instability of the far field vertical shear might occur when $\beta < 0.75$.

All free waves in the far field, both neutral and unstable, have real phase speeds less than $U_{01} = 0.15$, as shown in Fig. 12. There are two waves for each total wavenumber evolved from the barotropic and baroclinic Rossby waves in the absence of vertical shear. With vertical shear, the barotropic wave becomes bottom-intensified. Both retain their baroclinic or barotropic structure at low wavenumber. When the far field is locally stable, e.g. $\beta > F(U_{01} - U_{02})$, the phase speed range for the surface-intensified mode is $(U_1 + U_2)/2$ to U_1, and for the bottom-intensified mode, it is $-\infty$ to U_2. When the far field is unstable, both waves can have positive phase speeds. According to the semicircle theorem, jet instability phase speeds lie between the

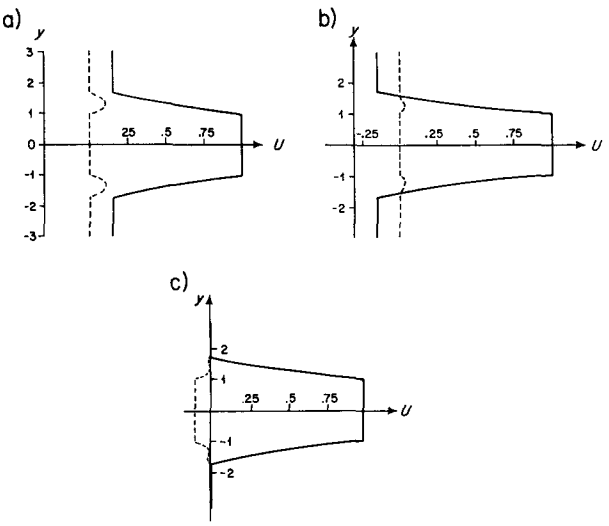

FIG. 11. Three modified eastward jets: (a) with positive vertical shear in Region III, (b) with negative vertical shear in Region III, (c) with a weak, westward undercurrent.

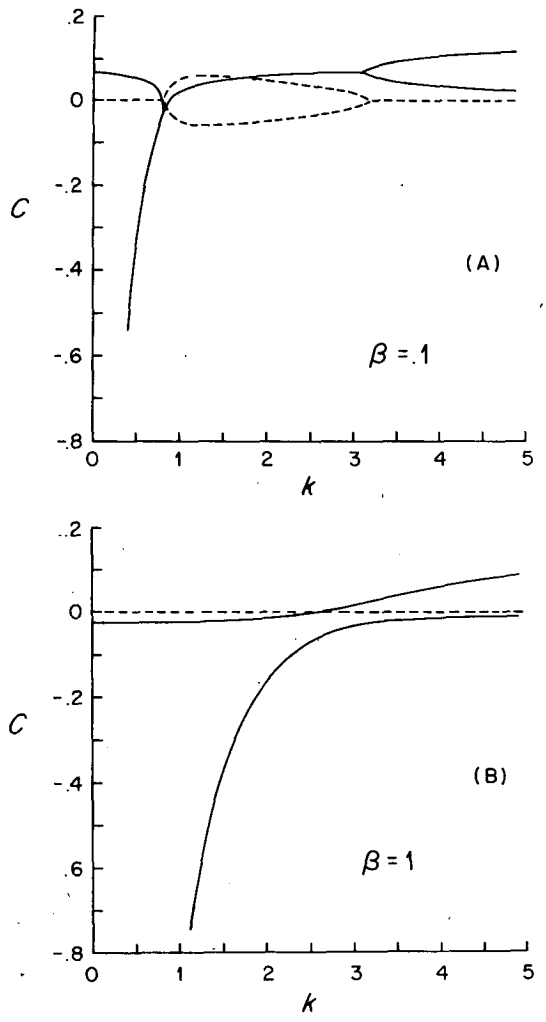

FIG. 12. Rossby wave dispersion relation for a fluid with two layers of equal depth and vertical shear $(U_1 - U_2) = 0.15$. The phase speed is shown as a function of k at $l = 0$ for (a) $\beta = 0.1$ and (b) $\beta = 1.0$. Notice that the phase speed is complex for $\beta = 0.1$. The solid curves are the real part and the dashed curves the imaginary part of c.

minimum flow speed, minus a small correction for β, and the maximum flow speed of the entire flow. Thus both free waves of the far field can be forced when $\beta < F(U_{01} - U_{02})$ but only one wave, the baroclinic or surface-intensified wave, can be forced when $\beta > F(U_{01} - U_{02})$.

The unstable waves for the jet were found. The stability diagram is shown in Fig. 13. It is much more complicated than Fig. 3 because radiating instabilities now exist for positive β. The two modes of the basic eastward jet are present and labelled as in Fig. 3. The trapped instabilities, indicated "ut", are vertical shear modes of the central jet and are nearly identical to the basic eastward jets' instabilities. Their real phase speeds decrease as β increases. Therefore the trapped modes become radiating at high β since it is now possible to force the free waves of the far-field when phase speeds fall beneath $U_{01} = 0.15$. This transition is indicated by the short-dashed curves, where the real and imaginary parts of the far field y-wavenumber are equal. Two additional, radiating modes were found which may be associated with the horizontal shear: the growth rates were so low, however, that full determination of vertical curves was not possible. These are not shown in Fig. 13.

The phase speed and growth rates at $\beta = 4$ are shown in Fig. 14. Growth rates fall off precipitously where the long-dashed curves in Fig. 13 are intersected: these were the neutral stability curves, $c_i = 0$, for the corresponding trapped modes of the basic jet (Fig. 3). However, growth rates do not tend to zero at the expected neutral curves but reach a low value in the regions indicated "rd" (radiating, destabilized). The waves in these regions of the stability diagram were neutral in Fig. 3, but are now destabilized by the jet: a large area of the stability diagram between the old neutral curves and the maximum β allowed by the necessary conditions for instability is destabilized. Thus, two types of radiating instability are found: jet instabilities that are trapped in the basic jet but satisfy

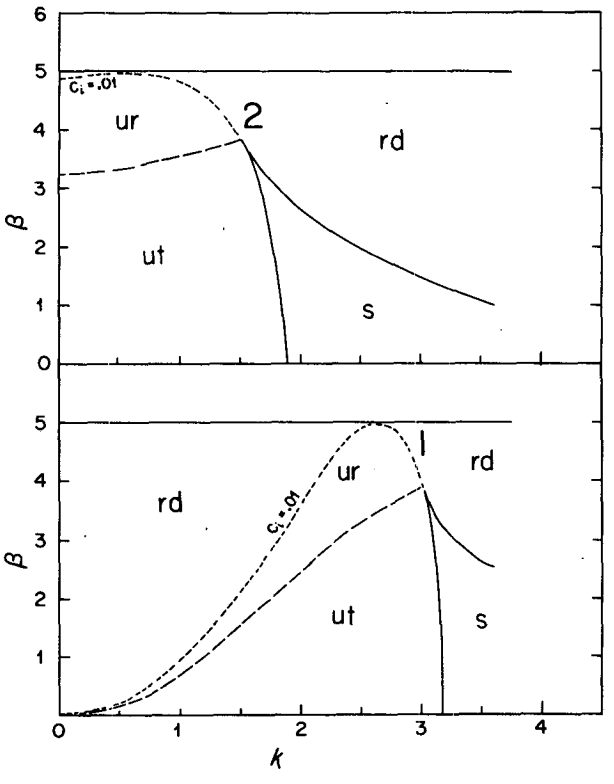

FIG. 13. Marginal stability curves in the β–k plane for the eastward jet with positive vertical shear in the far field, illustrated in Fig. 11a. The long-dashed curves are loci of $\mathrm{Re}(\hat{p}) = \mathrm{Im}(\hat{p})$. Notation is as in Fig. 3 with the addition of short-dashed curves labeled "c_i = .01" which separate radiating waves with rather large growth rates from those with uniformly low growth rates. The latter are referred to as destabilized Rossby waves and are labeled "rd" in the diagram.

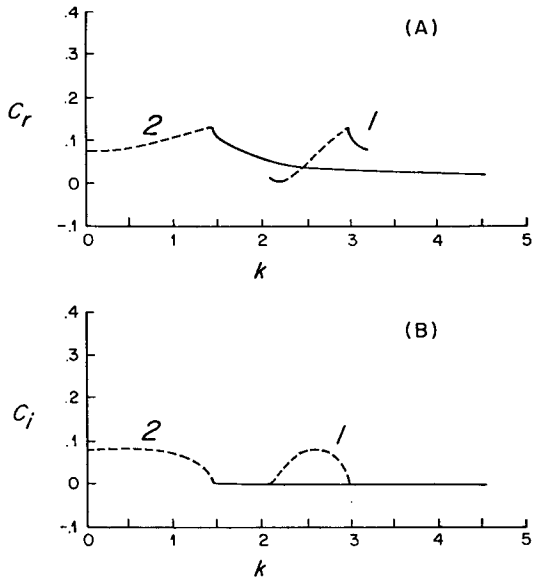

FIG. 14. (a) c_r and (b) c_i of the unstable modes for the eastward jet with positive vertical shear in the far field, at $\beta = 4$. c_i is small but nonzero at high k for Mode 2 and for low and high k for Mode 8.

the phase speed condition in this modified flow and a large range of formerly neutral, modified Rossby waves that are destabilized by the jet. The radiating instabilities do not involve the locally, baroclinically unstable waves of the far field (Region III): only the neutral waves of the far-field are "forced" by the jet instabilities.

The vertical structure of the radiating waves depends on which free waves are excited in the far field. All radiating waves of this particular flow excite only one wave, the wave that is baroclinic at low total wavenumber and surface-intensified at high total wavenumber. The total wavenumber turns out to be large for all radiating waves, so the far field structure is generally surface-intensified. A radiating wave is shown in Fig. 15. Its most important aspect, in addition to slow meridional decay, is surface-intensification. The Reynolds stress extremum in the surface layer is farther from the jet than in the lower layer where the unstable wave does not propagate well.

To summarize the results for the eastward jet with positive vertical shear in the exterior region, two basic modes are present in both nonradiating and radiating jets. Both modes have large growth rates and strongly trapped solutions which draw energy mainly from the vertical shear of the central jet. With positive vertical shear in Region III, some of these waves (those with $c_r < U_{01}$ and that are near the neutral curve) radiate. Waves with $c_r < 0.15$ and that fall on the neutral curve for the nonradiating jet are no longer stable but have small growth rates and connect to a large range of destabilized Rossby waves. Although there is baroclinic instability in Region III when $\beta < 0.75$, the locally baroclinically unstable waves are not involved in radiation of the central jet instabilities in this linear theory. Destabilized Rossby waves exist in the β–k plane wherever modified Rossby waves exist with phase speeds, c_r, that are determined by the jet if the necessary conditions for instability are satisfied. In other words,

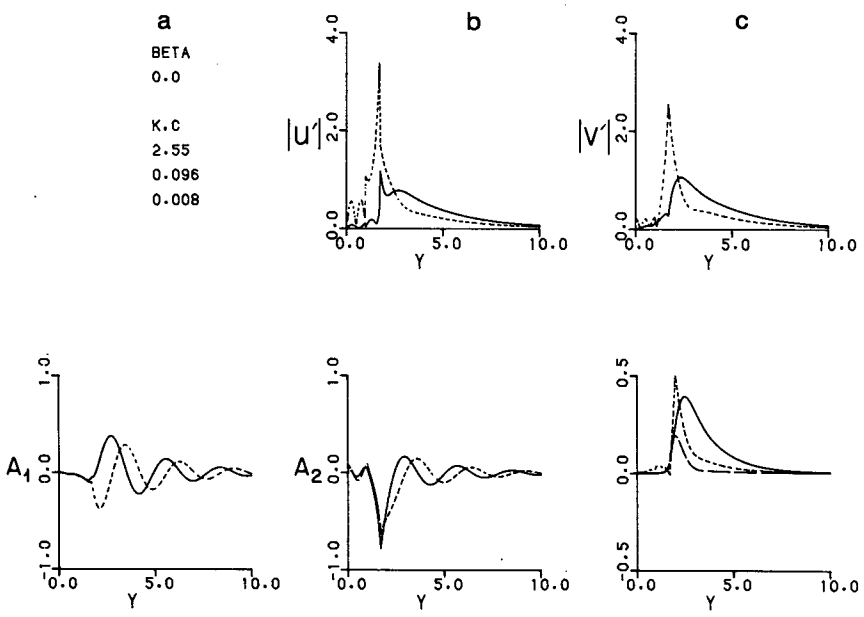

FIG. 15. A radiating eigenfunction at $\beta = 0$ for the jet with eastward vertical shear in the far field. (a) Real (solid) and imaginary (dashed) parts of the upper-layer amplitude and (b) lower-layer amplitude. (c) Upper-layer momentum flux (solid), lower-layer momentum flux (long dash) and heat flux (short dash), as in Fig. 8.

even though Rossby waves exist for all wavenumbers k, the jet does not select the phase speeds of the Rossby waves at high zonal wavenumber for destabilization. Thus there is a distinct short wave cutoff for the destabilized waves. The mechanism whereby a particular phase speed is selected for destabilization is unclear.

2) Eastward jet with negative vertical shear in the far field

A second, simple modification of the basic eastward jet is illustrated in Fig. 11b, where the only change from the basic jet is the inclusion of weak, negative vertical shear in the far field ($U_{01} = -0.15$). Again the far field can be baroclinically unstable for $\beta < 0.75$, although these instabilities are not linked to jet instabilities in the linear theory. The slight increase in horizontal shear in the upper layer increases the range of β which might be barotropically unstable, for $\beta < 4.04$. All free waves in the far field have negative phase speeds, as illustrated in Fig. 16 for $\beta = 0.1$ and 1.0. With negative shear, the formerly short, baroclinic Rossby waves become bottom-intensified and the short, barotropic Rossby waves become surface-intensified. When $\beta > F(U_{01} - U_{02})$, only the mode which is baroclinic at long wavelengths and bottom-intensified at short wavelengths has phase speeds between $U_{\min}$ and $U_{\max}$ of the whole profile, so it is probable that only this mode will be involved in jet radiation.

The stability diagram for this profile is shown in Fig. 17. It is divided into three parts, showing the two familiar modes and an additional mode. Modes 1 and 2 are vertical shear modes of the central jet and are stabilized at the β defined by the necessary conditions for instability. The additional mode is associated with the horizontal shear in the upper layer since it is sta-

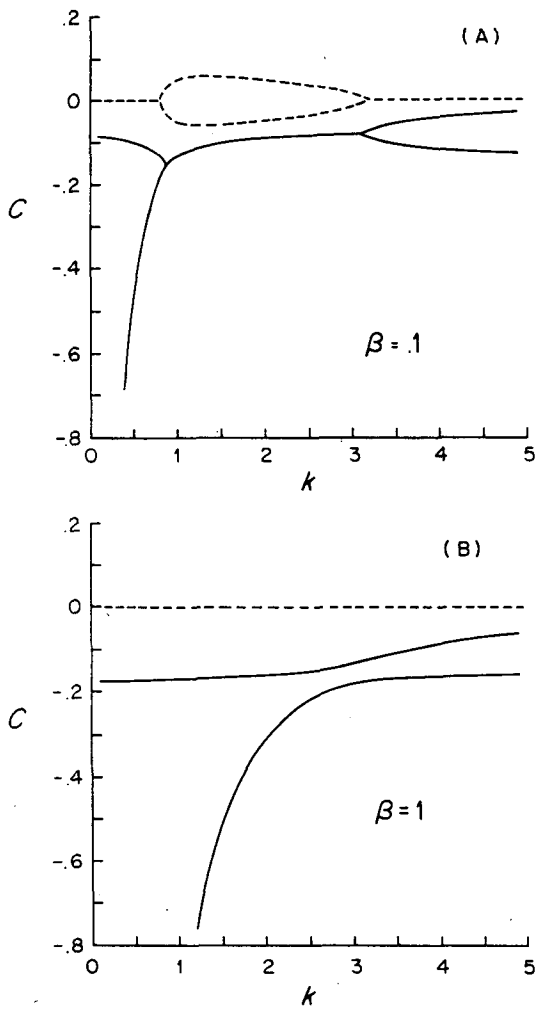

FIG. 16. Free-wave dispersion relations for a fluid with two layers of equal depth with vertical shear $(U_1 - U_2) = -0.15$. The phase speed is shown as a function of k for $l = 0$ for (a) $\beta = 0.1$ and (b) $\beta = 1.0$. The solid curves are the real part and the dashed curves the imaginary part of c.

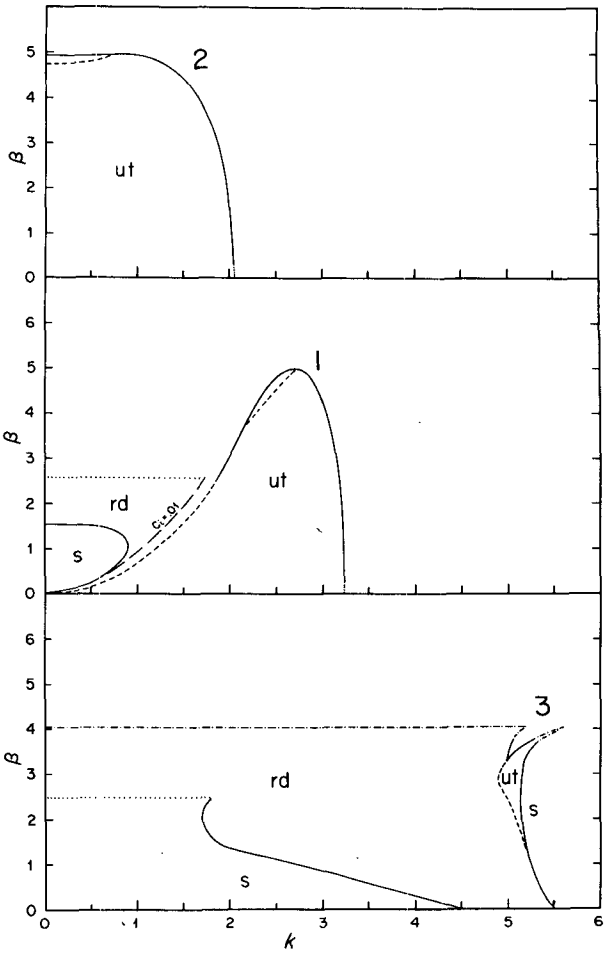

FIG. 17. Marginal stability diagram in the β–k plane for an eastward jet with negative vertical shear in the far field, as illustrated in Fig. 11b. Notation is as in Fig. 13 with the addition of dotted lines in Modes 1 and 3 which indicate that the radiating waves of Mode 1 at low β are continuous with radiating waves associated with Mode 3.

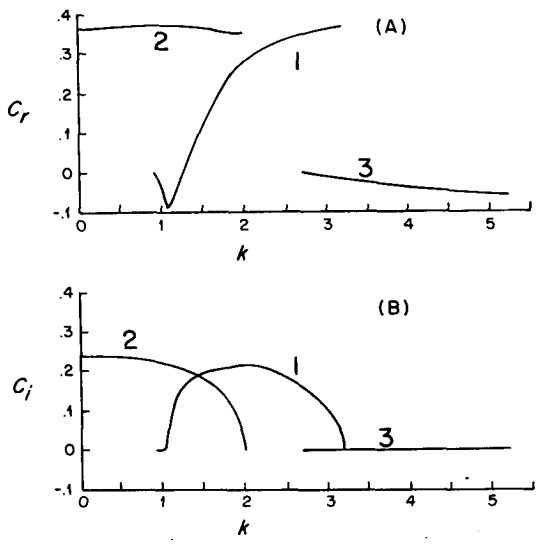

FIG. 18. (a) c_r and (b) c_i at $\beta = 1$ for the instabilities of the eastward jet with negative vertical shear in the far field. c_i of Mode 3 is small but nonzero.

bilized by β_c of about 4 and has the cusp at β_c associated with barotropic instability of these Rayleigh-type profiles (Talley, 1983). The occurrence of this mode results from increased horizontal shear in the upper layer.

As $\beta \rightarrow \beta_c$, the real phase speed of each mode tends to the minimum flow speed in the portion of the flow responsible for the instability. Thus, the phase speed of central-jet vertical shear modes tends to 0. The phase speed of upper-layer, horizontal shear modes tends to -0.15. Thus only the horizontal shear mode is expected to radiate. As seen in the stability diagram (Fig. 17), Mode 2, a vertical shear mode, does not radiate. Mode 1 is more complicated: at low β and low wavenumber, this mode incorporated a horizontal shear mode in the basic jet profile and does so here also. Hence there are radiating instabilities along this boundary, which was a neutral curve in the basic jet. Mode 3, the new mode, is a horizontal shear mode and has associated radiating instabilities.

The stability diagram is complicated by the long wave behavior of Modes 1 and 3: when β is 2, say, the radiating instabilities at low wavenumber are associated with the trapped instabilities of Mode 1, with a neutral curve just above $k = 3$. However, at $\beta = 3$, the low-wavenumber radiating instabilities connect with the trapped instabilities of Mode 3 at much higher wavenumber. This trade is indicated on the stability diagram by a dotted line. The orientation of the line is arbitrary but its end point at β and k of about 2.5 and 1.8 is well-defined. Thus, although both Modes 1 and 3 have associated destabilized Rossby waves (these radiating instabilities), there is only one set of radiating instabilities for this profile, apparently associated with the upper-layer horizontal shear.

Dispersion relations for the three modes are shown in Fig. 18. The long waves of Mode 1 and all of Mode 3 are radiating: the phase speeds are between -0.1 and 0. Hence from Fig. 16, it is clear that only the baroclinic or bottom-intensified wave in the far field will be involved in radiation. In fact, the total wavenumber in the far field, $k^2 + l_{\mathrm{Re}}^2$, is always large for the radiating

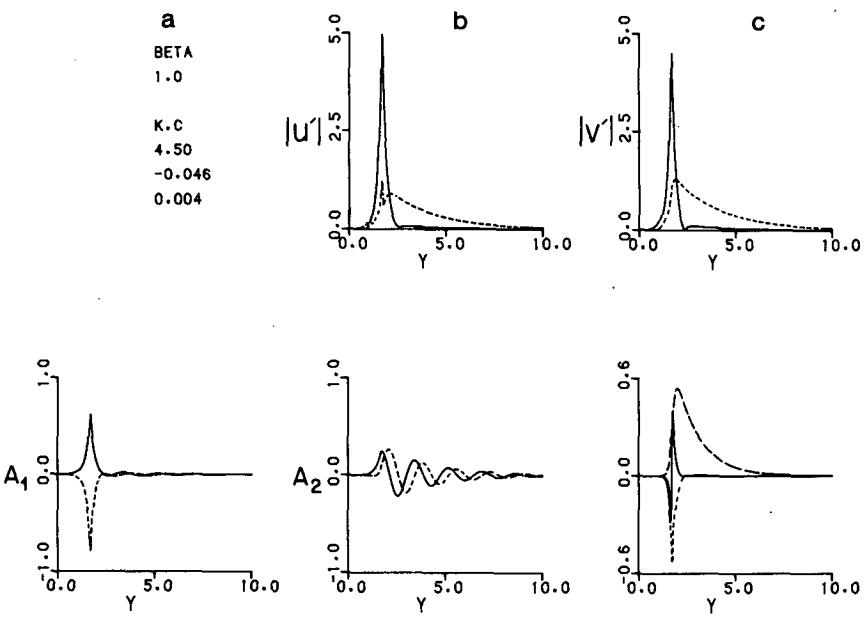

FIG. 19. A radiating eigenfunction at $\beta = 1$ for the jet with negative vertical shear in the far field. (a) Real (solid) and imaginary (dashed) parts of the upper-layer amplitude and (b) lower-layer amplitude. (c) Upper-layer momentum flux (solid), lower-layer momentum flux (long dash) and heat flux (short dash), as in Fig. 8.

waves so they are all bottom-intensified. A representative, radiating eigenfunction is shown in Fig. 19. This wave draws its energy from the horizontal shear of the upper layer but propagates in the lower layer in the far field. Hence its amplitude in the upper layer is large in the shear zone and negligible elsewhere, while its amplitude in the lower layer is large in the far field.

3) EASTWARD JET WITH WESTWARD UNDERCURRENT

The third, simple modification of the basic flow is to include a weak, westward undercurrent in the lower layer, $U_{12} = -0.1$, as illustrated in Fig. 11c. The free waves of the far field are once again baroclinic and barotropic Rossby waves. Radiation might be possible because the flow in the lower-layer jet is westward with respect to the far field. Evaluating the necessary conditions for instability, we find that vertical shear instability in the central jet might occur when $\beta < 5.5$; horizontal shear instability might be possible in the upper layer when $\beta < 2.94$; in the lower layer, horizontal shear instability and mixed instability, due to horizontal gradients of $\beta - FU_s$, might occur for $\beta < 5.5$.

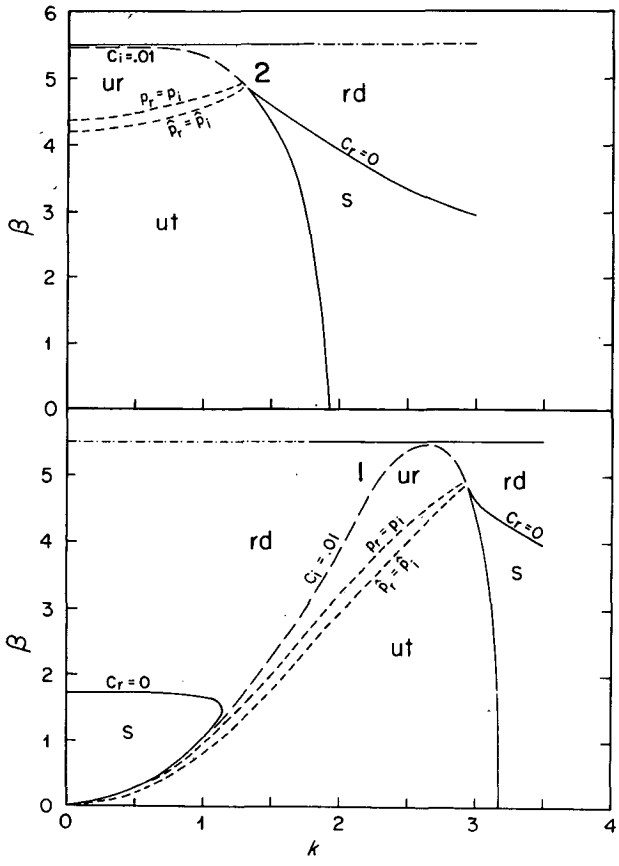

FIG. 20. As in Fig. 13 but for an eastward jet with weak westward undercurrent, as illustrated in Fig. 11c. Note that there are now dashed curves for both p and $\hat{p}$: both free waves are forced in the far field.

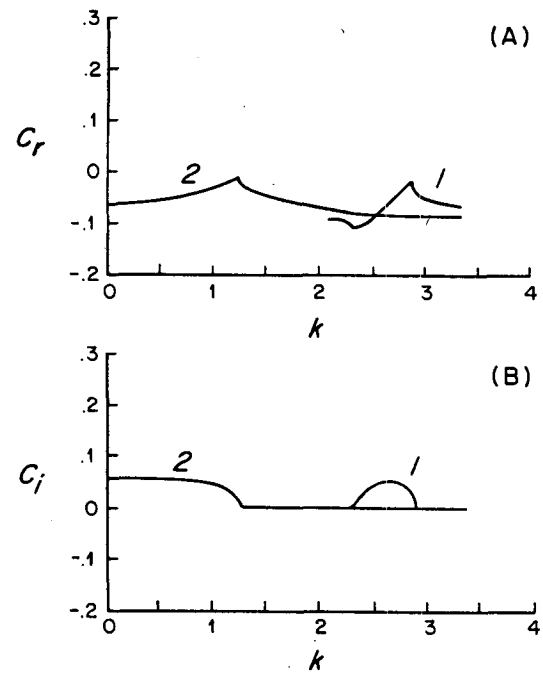

FIG. 21. (a) c_r and (b) c_i at $\beta = 5$ for the unstable modes of eastward jet with weak westward undercurrent. Again, the very small values of c_i shown here are nonzero.

Radiation may be possible if unstable waves have negative phase speeds. As β increases to the appropriate β_c for each mode, the phase speed decreases to the minimum speed of its associated part of the flow profile. Each unstable mode is associated with a particular part of the profile: the vertical shear modes with the central jet flow, which has a range of -0.1 to 1, and the horizontal shear modes with the upper layer velocity, which has a range of 0 to 1, and with the lower layer flow, which has a range of -0.1 to 0. Thus for this profile, we would expect the vertical shear modes of the central jet and the lower-layer horizontal shear mode to be much more likely to radiate than the upper-layer horizontal shear mode.

The stability diagram is shown in Fig. 20. Once again, the slight modification of the jet has left Modes 1 and 2 nearly unaltered. There are no separate horizontal shear modes associated with either the upper or lower layers, although the long wave behavior of Mode 1 is influenced by the presence of horizontal shear, just as for the jets already discussed. The necessary condition for vertical shear instability is sufficient as before. There are radiating instabilities near the neutral curves of the basic jet (Fig. 4) on the long wave side of Mode 1 and at high β for both modes. As before, the neutral waves themselves are destabilized and there is a large range of formerly neutral, far-field Rossby waves that are now unstable. The stability diagram shows no short-wavenumber cutoff for these ra-

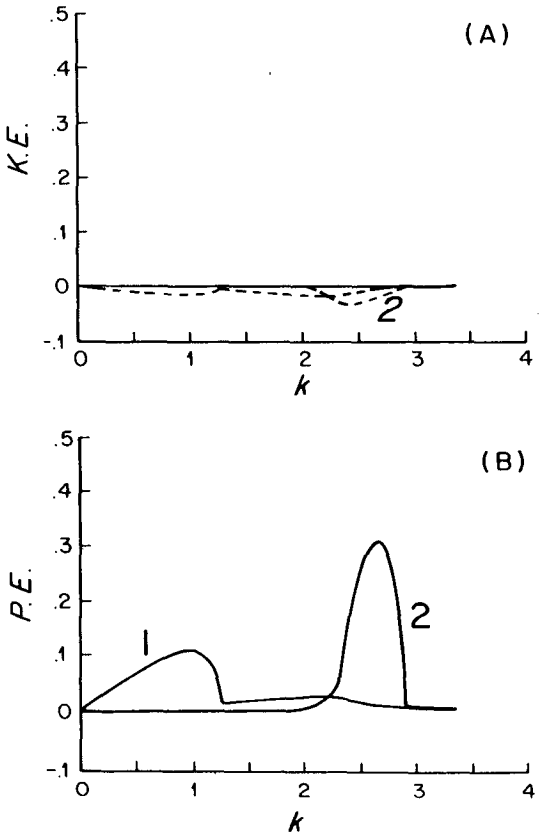

FIG. 22. (a) Transfer of energy from the mean flow of the upper layer (dashed) and lower layer (solid) and (b) transfer of mean-flow potential energy to the perturbations, at $\beta = 5$, for the eastward jet with weak westward undercurrent.

diating waves because growth rates are very low and the instabilities were difficult to find at higher k. However, short-wave cutoffs were found for the radiating instabilities of the other jets so there is no reason not to expect a cutoff here.

Dispersion relations are shown in Fig. 21 at $\beta = 5$. All instabilities at $\beta = 5$ radiate: their phase speeds are negative and they satisfy the definition of radiation. Here we can see graphically one difference between the radiating instabilities that are basically unstable modes of the jet and those that are destabilized Rossby waves: the growth rates of the basic instabilities are good-sized although all are radiating while the growth rates of the destabilized Rossby waves are very small.

The energy transfers at $\beta = 5$ are shown in Fig. 22. This β is considerably in excess of the β_c associated with the upper-layer horizontal shear instabilities, so the perturbations grow at the expense of the mean-flow potential energy. Indeed, all energy transfer to the perturbations is from the potential energy of the mean flow while the perturbations actually lose kinetic energy.

Radiating instabilities for this profile involve both the barotropic and baroclinic Rossby waves in the far field. Since the two waves have different meridional wavenumbers, the resulting eigenfunction alternates between surface- and bottom-intensification. Fig. 23 shows this behavior. Note that the eigenfunction is largest in the jet center, probably because the energy source is the vertical shear of the central jet. Outside the jet, the momentum flux also alternates between surface- and bottom-intensification while the heat flux is slightly negative but small.

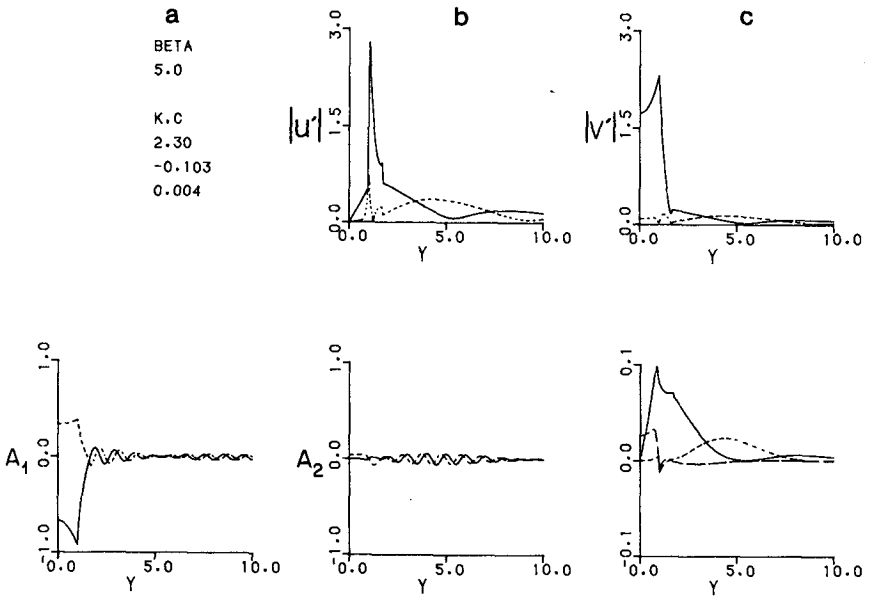

FIG. 23. As in Fig. 19 but at $\beta = 5$ for the eastward jet with weak westward undercurrent.

c. *The effect of selected parameter changes*

There are a large number of parameters in the two-layer jet, which affect the relative importance of barotropic and baroclinic instability and the structure of the instabilities. Systematic changes in a basic profile were made in the previous section to understand the circumstances in which a simple jet radiates. A thorough exploration of parameters is not made here because there are too many possibilities. Discussed briefly here are 1) the effect on the radiating modes of zonal boundaries far from the jet, 2) the effect of a weak eastward jet in the lower layer which decreases the central jet vertical shear, thus increasing the barotropy, 3) changing the width of the shear zones, which affects the amount of kinetic energy transfer and the number of barotropic instability modes and 4) changing F, which affects the amount of potential energy transfer and the number of baroclinic instability modes.

1) Effect of zonal boundaries

Imposition of zonal boundaries at a large distance compared with the jet width has no effect on the trapped instabilities since their influence does not extend far beyond the jet. However, boundaries change the behavior of radiating instabilities which have large meridional decay scales by setting up standing waves.

Figure 24a is an expanded version of the imaginary part of the phase speed of the radiating mode associated with Mode 1 in Fig. 20. No boundaries were used in the calculations of the previous section. When boundaries are included at $H = \pm 100$, there are well defined ranges of zero c_i (Fig. 24b). Each lobe of positive c_i corresponds to a separate standing mode of the entire channel. A similar observation of the effect of boundaries on radiating Kelvin–Helmholtz instabilities was made by Lindzen and Rosenthal (1976): when fluid above and below a shear layer was stratified so that internal waves could be supported, radiating instabilities were observed. With lateral boundaries, the dispersion relation was modified in the same way as in the present case.

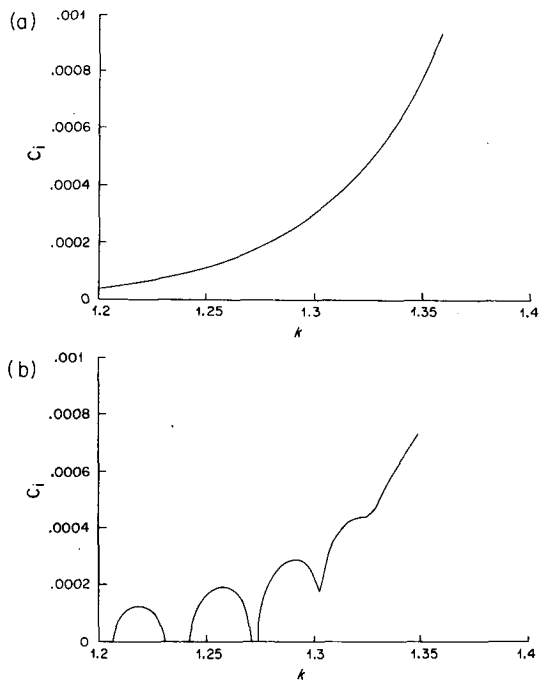

FIG. 24. c_i for long, radiating waves of Mode 1 (Fig. 20) for (a) an infinite β-plane and (b) a channel with walls at $H = \pm 100$.

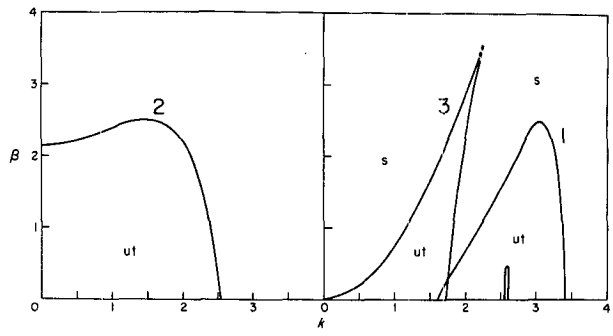

FIG. 25. Marginal-stability curves in the β–k plane for a jet identical to Fig. 2 but with $U_{12} = 0.5$. Only positive β is shown.

2) Effect of variable vertical shear in the central jet

Changes in the vertical shear in the central jet should shift the relative importance of baroclinic and barotropic instability. Fig. 25 is the stability diagram for a jet identical to Fig. 2 but with $U_{12} = 0.5$ instead of 0. The decrease in vertical shear in the central jet from $U_1 - U_2 = 1.0$ to $U_1 - U_2 = 0.5$ results in an obvious decrease in importance of the vertical shear modes. It also results in separation of the main horizontal shear mode from the vertical shear Mode 1. There is a much larger proportion of kinetic-energy transfer to this horizontal shear mode than to Modes 1 and 2, although the mean-flow potential energy is still the dominant source of energy. Modes 1 and 2 were identified as vertical shear modes by their associated β_c and the similarity of their marginal stability curves to those of the first two baroclinically unstable modes for a channel. The marginal curve of Mode 3 terminates at the β_c predicted for barotropic instability of the upper layer and has the cusp at β_c typical of horizontal shear modes.

3) Effect of narrower shear zones

Talley (1983) discussed the effect of narrower shear zone widths ($D - 1$), and hence increased horizontal shear, on barotropic instabilities. A top-hat jet is un-

stable for all β and k. As shear zone widths increase, instabilities are restricted to smaller ranges of β and k. The number of barotropically unstable modes also decreases, although there is always at least one unstable mode no matter how large D becomes. Such behavior should extend to the horizontal-shear modes of two-layer jets. Vertical-shear modes should be much less affected by varying shear-zone widths.

We examine briefly the effect of narrowing the shear zones of the jet discussed in the immediately preceding section, which had $U_{12} = 0.5$. The shear zone widths are decreased from 0.7 to 0.5. The stability diagram is shown in Fig. 26. The vertical shear modes (1 and 2) are nearly unaffected. However, β_c for the horizontal shear mode (3) is now much higher and there are two new horizontal shear modes. This is in keeping with the results of Talley (1983) and strengthens the identification of Mode 3 as a horizontal shear mode. Although the energy transfers are not shown, it was found that the vertical shear modes were dominated by potential energy transfers; the source of energy for the horizontal shear modes for $\beta < 2.5$ was largely potential but nearly all kinetic for $\beta > 2.5$.

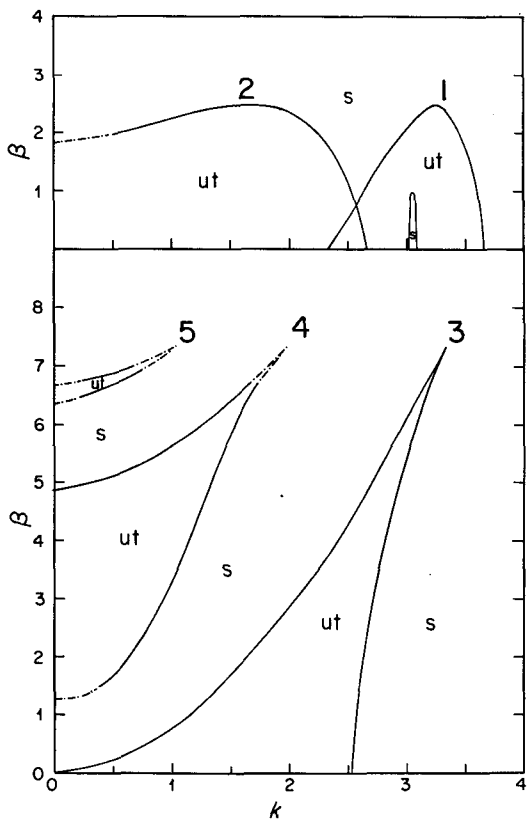

FIG. 26. Marginal-stability curves for a jet identical to Fig. 2 but with $U_{12} = 0.5$ and $D = 1.5$ rather than 1.7. There are two vertical-shear modes (1 and 2) and three horizontal-shear modes (3, 4 and 5).

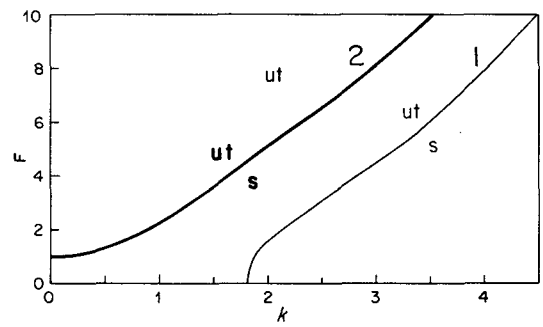

FIG. 27. Marginal-stability curves in the F–k plane for the basic jet, Fig. 2, at $\beta = 0$. The modes are the same as the two modes of Fig. 3.

4) EFFECT OF CHANGES IN F

Hart (1974), Holland and Haidvogel (1980) and Orlanski (1969) examined the effect of changing stratification on baroclinic jets, so this discussion is brief. As the density contrast between the layers is reduced, F increases, the interface becomes more pliant and the flow becomes more baroclinically unstable. When F is zero, there is no baroclinic instability. The basic jet profiles, at $F = 5$, had two unstable modes. Mode 2 was a vertical shear mode while Mode 1 was composed of a horizontal- and a vertical shear mode which separated when $U_{12} = 0.5$. The stability diagram for the two modes at $\beta = 0$ as a function of F and k is shown in Fig. 27. Mode 1 is unstable for all F: its existence at low F can only be due to horizontal shear, strengthening the characterization of Mode 1 as a combined horizontal–vertical shear mode. Mode 2 is stable at low F: it is solely a vertical shear mode. (Note that there is only one horizontal shear mode when $D = 1.7$ for a barotropic jet, so only one horizontal shear mode is found here.) A similar result was found by Hart (1974): he found instabilities even at very low values of F, due entirely to the horizontal shear of the upper layer jet.

d. Model summary

The linear stability of baroclinic, zonal jets on the β-plane was explored: it was found empirically that it was possible to predict the existence of radiating solutions based on the Rossby-wave dispersion relation in the far field of the jet and the necessary conditions for instability (which were sufficient for profiles considered here although they are not guaranteed to be sufficient for general cases). Because the flows had vertical and horizontal shear, both baroclinic and barotropic instability were possible. Identifiable horizontal and veritical shear instabilities were found, each for

parameter ranges given by the necessary condition for instability.

The basic eastward jet has two unstable modes, which were identified as the two gravest, cross-jet, baroclinically unstable modes. The gravest mode, Mode 1, also incorporated an upper-layer horizontal shear mode which strongly affected the long wave behavior, particularly the shape of the neutral curve and the phase speeds. (The horizontal shear mode separated from Mode 1 when an eastward jet was gradually introduced in the lower layers.) All instabilities of the eastward jet were trapped and were predominantly vertical shear modes. In contrast, the westward jet basically had two modes, but (1) horizontal shear instability was more important and (2) there were radiating instabilities associated with two sources of energy, the upper-layer kinetic energy and the potential energy of the central jet. The growth rates of the radiating instabilities were comparable to those of the trapped instabilities.

The instabilities of the eastward jets with small modifications were very similar to those of the basic, eastward jet with the important addition of large ranges of unstable, radiating waves. These instabilities were separated into 1) unstable waves of the basic, eastward jet which radiate due to modification of the jet structure and 2) a large new class of unstable solutions which are basically Rossby waves of the far field, destabilized by the jet. Growth rates of radiating instabilities 1) and destabilized Rossby waves 2) are lower than growth rates of trapped instabilities (McIntyre and Weissman, 1978). However, growth rates of radiating instabilities were found to depend strongly on the allowed range of phase speeds for radiation: hence, the radiating instabilities of predominantly eastward jets had very low growth rates while the growth rates of radiating instabilities of the westward jet were comparable to those of trapped instabilities.

The energy source for all instabilities was, as expected, a mixture of mean-flow potential and kinetic energy. For the particular jets considered here, baroclinic instability was the dominant mechanism even for modes identified with the horizontal shear. If the necessary conditions for baroclinic and barotropic instability were both met, there was energy transfer to the perturbations by both mechanisms. If the necessary conditions for, say, barotropic instability were not satisfied but those for baroclinic instability were, the perturbations gained energy from the mean-flow potential energy and lost it to the mean-flow kinetic energy.

The horizontal structure of the instabilities depended on the energy source: if it was the vertical shear, maximum amplitude occurred in the jet center while if it was the upper-layer horizontal shear, maximum amplitude occurred in the shear zone. Outside the jet, the vertical structure of trapped waves was usually barotropic. The vertical structure of radiated waves depended entirely on how the phase speed condition was satisfied, i.e., which of the two free waves was forced.

4. Gulf Stream comparison

One motivation for the study of radiating instabilities was the structure of the eddy energy field of the Gulf Stream. The observed, highly energetic eddy field in the Gulf Stream and its broad decay to the south can only be due to instabilities of the Gulf Stream and its recirculation. Two possible sources of the observed eddy field are Gulf Stream rings (Flierl, 1977), which result from Gulf Stream instabilities, and the finite amplitude extension of radiating instabilities. It is assumed in the following comparison that radiating instabilities are the eddy source and then seen to what extent this assumption is consistent. However, it is difficult to compare linear stability results with observed fluctuations because the appropriate basic flow is unknown. The approach here is to use the gross observed characteristics of the energy distribution to suggest the correct basic flow. If the model is appropriate, it should then yield reasonable frequencies, wavenumbers, Reynolds stress and heat flux for the eddy field.

We begin with a short summary of the observations, followed by a comparison of model and results. Observations made along 55°W in the POLYMODE Experiment and at the MODE site are used. Schmitz (1978, 1980, 1982) has published the vertical and meridional distributions of mean flow, kinetic energy and Reynolds stress along 55°W. There were no moorings directly in the Gulf Stream except at 4000 m. The mean flow south of the mean Gulf Stream axis was characterized by nearly barotropic eastward flow at 37°50′N, nearly barotropic westward flow at 36°N and weak flow of indeterminate sign south of 35°N. At 4000 m beneath the mean Gulf Stream axis there was a westward flow, although it is not clear that the instantaneous westward flow was beneath the instantaneous Gulf Stream.

The vertical distributions of eddy kinetic energy at 37°30′N, 55°W and at the MODE site (28°N, 70°W) were compared by Schmitz (1978). The POLYMODE mooring is about 200 km and the MODE mooring is about 800 km from the Gulf Stream. Mesoscale fluctuations (50 to 100 days) were weakly surface-intensified and decayed quickly away from the Gulf Stream maintaining their vertical structure. Secular fluctuations (100 to 1000 days) decayed much more slowly and became strongly surface-intensified away from the Gulf Stream.

The momentum flux along 55°W (Schmitz, 1982) was positive south of the Gulf Stream and appeared to cross zero in the Gulf Stream, although moorings were not placed in the Gulf Stream. The maximum momentum flux occurred farther south in the ther-

mocline than in the deep water. The momentum flux was antisymmetric with respect to the current axis: although data to support this at 55°W are only available at 400 m, it is true at shallower depths in the Kuroshio (Schmitz, 1982).

Hogg (personal communication, 1982) calculated the heat flux $\overline{v'T'}$ for POLYMODE Array 2 at 600 and 4000 m. The abyssal heat flux was negative and small throughout the array. The thermocline heat flux was large and southward at 37°30'N, in the westward mean flow south of the Gulf Stream. South of 35°N, the thermocline heat flux was nearly zero.

A basic flow must be chosen for the model in order to compare it with data. The observed mean flow is not necessarily the best choice of basic state since it has already been altered by instabilities. Thus the structure of observed fluctuations is used to define a reasonable basic flow. The fast meridional decay of the mesoscale fluctuations (Schmitz, 1978) leads us to identify them as trapped disturbances. Weak surface-intensification of mesoscale disturbances was observed: if the two-layer model used here had had a shallower surface layer, the trapped instabilities would have been usually surface-intensified in the far field rather than barotropic. Since the trapped modes of all models had barotropic structure outside the jet, no further information about the basic state is obtained from the mesoscale fluctuations. The secular-scale fluctuations decayed much more slowly and became strongly surface-intensified far from the Gulf Stream: they can be identified as radiating instabilities. Of the models considered, the model with weak eastward vertical shear in the ocean interior and the one with a westward undercurrent produced surface-intensified disturbances in the far field.

The momentum flux in the far field for radiating instabilities in the model with eastward vertical shear in the ocean interior was surface-intensified (Fig. 15), antisymmetric and had a maximum farther south in the upper layer, just as in the observations (Schmitz, 1982; Fig. 2). Thus on the basis of Schmitz's (1978) kinetic energy analysis and his momentum flux distribution (Schmitz, 1982), the best model of those few considered here has weak, positive vertical shear in the far field. A subtropical gyre with weak eastward velocities south of the Gulf Stream and an intense westward recirculation is conceivable in terms of inertial circulation models (cf. Veronis, 1966) and observations (Reid, 1978) but differs from the more conventional view of broad westward flow south of the Gulf Stream (Stommel *et al.*, 1978; Worthington, 1976).

The present models cannot produce the observed large, southward heat flux in the westward mean flow, south of the Gulf Stream. This flow is an important feature of all detailed observations and circulation models and is lacking in the present model. The model's simplicity must be reappraised in light of the observed heat flux and the necessity for weak eastward flow in the ocean interior (in order to produce surface-intensified fluctuations using this model). A possible scenario is that the eastward Gulf Stream is unstable to fluctuations that are strongly trapped meridionally. The momentum flux divergence due to these waves sets up westward side lobes that are nearly barotropic because the tails of the trapped waves outside the Gulf Stream are nearly barotropic. The new mean flow may now be unstable to radiating modes because of the intense westward recirculation. These eddy-driven flows may themselves be unstable to instabilities with lower growth rates, such as the radiating instabilities that we seek. Certainly if slowly growing perturbations can draw energy from the flow despite the presence of more unstable waves, the relevant basic flow would have to include the effect of the most unstable waves.

Of course it is necessary to understand the nonlinear development of a full spectrum of waves, including both high-growth-rate trapped instabilities and weaker radiating modes, in order to make a truly significant comparison of the model and observations. Questions which must be answered are whether the weaker instabilities are capable of growth alongside the most unstable waves and what the final meridional distribution of unstable waves is. Perhaps the simplest conclusion to be reached from this model is that when conditions allow instabilities to radiate, they will, and that as a result, westward flows are much more likely to radiate energy far into the ocean interior than eastward flows.

Acknowledgments. The guidance provided by Joseph Pedlosky, who suggested the problem, was invaluable. I also thank William Schmitz, Nelson Hogg, Glenn Flierl and Dale Haidvogel for useful conversations. Comments by the anonymous referees were very helpful. The work was part of a Ph.D. thesis in the MIT/WHOI Joint Program in oceanography and was supported by a grant from the National Science Foundation's Office of Atmospheric Science to the Woods Hole Oceanographic Institution and by Grant OCE-8117700 from the National Science Foundation's Office of Ocean Sciences to Oregon State University.

APPENDIX

Perturbation Energy Equation

The perturbation energy equation is obtained by multiplying the potential vorticity equation for each layer (1) by ϕ_n and the depth of the layer, summing and then integrating over x and y. The summed and x-averaged energy equation is

$$\frac{\partial \overline{E(\phi)}}{\partial t} - \frac{\partial}{\partial y}\overline{\phi_1\left(\frac{\partial}{\partial t} + U_1\frac{\partial}{\partial x}\right)\phi_{1y} + \phi_2\left(\frac{\partial}{\partial t} + U_2\frac{\partial}{\partial x}\right)\phi_{2y}}$$
$$= \frac{dU_1}{dy}\overline{\phi_{1x}\phi_{1y}} + \frac{dU_2}{dy}\overline{\phi_{2x}\phi_{2y}} + F(U_1 - U_2)\overline{\phi_1\phi_{2x}}, \quad \text{(A1)}$$

where the overbar denotes the x-average. The averaged perturbation energy is

$$\overline{E(\phi)} = \frac{F}{2}\overline{(\phi_1 - \phi_2)^2} + \frac{1}{2}\sum_{n=1}^{2}[\overline{(\phi_{nx})^2} + \overline{(\phi_{ny})^2}].$$

If U_n and dU_n/dy are continuous, integration in y eliminates the bracketed term in (12) since $\phi_{nx} = 0$ at $y = \pm H$. When U_n and U_{ny} are discontinuous, however, this term may be nonzero. Suppose there are discontinuities in U_n and dU_n/dy at $y = y_0$. Integrating the bracketed terms in (A1) from one channel wall to the other yields the term

$$\left[\phi_1\left(\frac{\partial}{\partial t} + U_1\frac{\partial}{\partial x}\right)\phi_{1y} + \phi_2\left(\frac{\partial}{\partial t} + U_2\frac{\partial}{\partial x}\right)\phi_{2y}\right]_{y=y_0}, \quad \text{(A2)}$$

i.e., the jump in the bracketed quantity at $y = y_0$. Expressing ϕ_n in terms of normal modes, $\phi_n = [\Phi_n(y)e^{ik(x-ct)} + \text{c.c.}]/2$, the jump is evaluated using the match conditions for ϕ_1 and ϕ_2 at $y = y_0$. Denote the velocities north of the jump as U_n^+ and those south of it by U_n^-. Then (A2) becomes

$$\frac{ike^{2kct}}{4}\sum_{n=1}^{2}\frac{(U_n^+ - U_n^-)}{|U_n^+ - c|^2}\left\{|\Phi_n^+|^2\frac{dU_n^+}{dy}c + \Phi_n^{+*}\frac{d\Phi_n^+}{dy}(U_n^+ - c)^2 - \text{c.c.}\right\}$$

where the asterisk denotes complex conjugation. This can be rewritten in delta function form

$$\frac{ike^{2kct}}{4}\sum_{n=1}^{2}\int_{-H}^{H}dy\left\{|\Phi_n^+|^2\frac{dU_n^+}{dy}c + \Phi_n^{+*}\frac{d\Phi_n^+}{dy}(U_n^+ - c)^2 - \text{c.c.}\right\}\frac{(U_n^+ - U_n^-)}{|U_n^+ - c|^2}\delta(y - y_0).$$

Thus (A2) is basically a delta-function addition to the energy transfer term $(-\overline{u'v'})dU/dy$ in the perturbation energy equation. If $U_n^+ = U_n^-$, this term disappears because dU/dy no longer has delta-function behavior at $y = y_0$ and the energy equation is

$$\int_{-H}^{H}\frac{\partial \overline{E(\phi)}}{\partial t}dy = \int_{-H}^{H}\overline{\phi_{1x}\phi_{1y}}\frac{dU_1}{dy} + \overline{\phi_{2x}\phi_{2y}}\frac{dU_2}{dy} + F(U_1 - U_2)\overline{\phi_1\phi_{2x}}dy.$$

If, however, the kinetic energy transfers are written in the form $U\partial(\overline{u'v'})/\partial y$ there will be delta-function contributions even when U_n is continuous and dU_n/dy is discontinuous, in which case

$$\int_{-H}^{H}dy\overline{U_{ny}\phi_{nx}\phi_{ny}} = -[\overline{U_n\phi_{nx}\phi_{ny}}]_{y_0} - \int_{-H}^{H}dyU_n\frac{\partial}{\partial y}(\phi_{nx}\phi_{ny}).$$

Rewriting ϕ in normal mode form, $\phi_n(y)e^{ik(x-ct)}$, and applying the matching conditions, Eq. (A1) becomes

$$\int_{-H}^{H}dy\frac{\partial \overline{E(\phi)}}{\partial t} = \frac{ke^{2kct}}{2}\sum_{n=1}^{2}\left\{c_i\int_{-H}^{H}dy\frac{U_n|\Phi_n|^2}{|U_n - c|^2}(U_{ny}^- - U_{ny}^+)\delta(y - y_0) - \frac{i}{2}\int_{-H}^{H}dyU_n\frac{\partial}{\partial y}(\Phi_n\Phi_{ny}^* - \text{c.c.})\right\} + \frac{ik}{4}e^{2kct}F(U_1 - U_2)(\Phi_1\Phi_2^* + \Phi_1^*\Phi_2),$$

where the unsuperscripted U_n and Φ_n are the continuous values of U_n and Φ_n. There is clearly a contribution to the convergent Reynolds stresses from the profile break because $\overline{u'v'}$ is not continuous there.

REFERENCES

Bernstein, R. L., and W. B. White, 1977: Zonal variability in the distribution of eddy energy in the mid-latitude North Pacific Ocean. *J. Phys. Oceanogr.*, **7**, 123–126.

Dantzler, H. L., 1977: Potential energy maxima in the tropical and subtropical North Atlantic. *J. Phys. Oceanogr.*, **7**, 512–519.

Dickinson, R. E., and F. J. Clare, 1973: Numerical study of the unstable modes of a hyperbolic-tangent barotropic shear flow. *J. Atmos. Sci.*, **30**, 1035–1049.

Edmon, H. J., B. J. Hoskins and M. F. McIntyre, 1980: Eliassen–Palm cross sections for the tropopause. *J. Atmos. Sci.*, **37**, 2600–2616.

Flierl, G. R., 1977: The application of linear quasigeostrophic dynamics to Gulf Stream rings. *J. Phys. Oceanogr.*, **7**, 365–379.

——, V. D. Larichev, J. C. McWilliams and G. M. Reznik, 1980: The dynamics of baroclinic and barotropic solitary eddies. *Dyn. Atmos. Oceans*, **5**, 1–41.

Fritts, D. C., 1982: Shear excitation of atmospheric gravity waves. *J. Atmos. Sci.*, **39**, 1936–1952.

Garcia, R. V., and R. Norscini, 1970: A contribution to the baroclinic instability problem. *Tellus*, **22**, 239–250.

Gent, P. R., 1974: Baroclinic instability of a slowly varying zonal flow. *J. Atmos. Sci.*, **31**, 1983–1994.

——, 1975: Baroclinic instability of a slowly varying zonal flow: Part 2. *J. Atmos. Sci.*, **32**, 2094–2102.

Haidvogel, D. B., and W. R. Holland, 1978: The stability of ocean currents in eddy-resolving general circulation models. *J. Phys. Oceanogr.*, **8**, 393–413.

Hart, J. E., 1974: On the mixed stability problem for quasi-geostrophic ocean currents. *J. Phys. Oceanogr.*, **4**, 349–356.

Holland, W. R., and D. B. Haidvogel, 1980: A parameter study of the mixed instability of idealized ocean currents. *Dyn. Atmos. Oceans*, **4**, 185–215.

Howard, L. N., 1961: Note on a paper of John Miles. *J. Fluid Mech.*, **10**, 509–512.

Lindzen, R. S., and A. J. Rosenthal, 1976: On the instability of Helmholtz velocity profiles in stable stratified fluids when a lower boundary is present. *J. Geophys. Res.*, **81**, 1561–1571.

McIntyre, M. E., and M. A. Weissman, 1978: On radiating instabilities and resonant overreflection. *J. Atmos. Sci.*, **35**, 1190–1196.

Orlanski, I., 1969: The influence of bottom topography on the stability of jets in a baroclinic fluid. *J. Atmos. Sci.*, **26,** 1216–1232.

Pedlosky, J., 1964a: The stability of currents in the atmosphere and the ocean: Part I. *J. Atmos. Sci.*, **21,** 201–219.

——, 1977: On the radiation of meso-scale energy of the mid-ocean. *Deep-Sea Res.*, **24,** 591–600.

——, 1979: *Geophysical Fluid Dynamics.* Springer-Verlag, 624 pp.

Philander, S. G. H., 1978: Forced oceanic waves. *Rev. Geophys. Space Phys.*, **16,** 15–46.

Rayleigh, Lord, 1879: On the instability of jets. *Scientific Papers,* **1,** 361–371, Dover, 1964.

Reid, J. L., 1978: On the mid-depth circulation and salinity field in the North Atlantic Ocean. *J. Geophys. Res.*, **83,** 5063–5067.

Richardson, P. L., 1983: Eddy kinetic energy in the North Atlantic from surface drifters. *J. Geophys. Res.*, **88,** 4355–4367.

Schmitz, W. J., 1978: Observations of the vertical distribution of low frequency energy in the western North Atlantic. *J. Mar. Res.*, **36,** 295–310.

——, 1980: Weakly depth-dependent segments of the North Atlantic circulation. *J. Mar. Res.*, **38,** 111–133.

——, 1982: A comparison of the mid-latitude eddy fields in the western North Atlantic and North Pacific Oceans. *J. Phys. Oceanogr.*, **12,** 208–210.

——, P. P. Niiler, R. L. Bernstein and W. R. Holland, 1982: Recent long-term moored instrument observations in the western North Pacific. *J. Geophys. Res.*, **87,** 9425–9440.

Stommel, H., P. Niiler and D. Anati, 1978: Dynamic topography and recirculation of the North Atlantic. *J. Mar. Res.*, **36,** 449–468.

Talley, L. D., 1983: Radiating barotropic instability. *J. Phys. Oceanogr.*, **13,** 972–987.

Tung, K. K., 1981: Barotropic instability of zonal flows. *J. Atmos. Sci.*, **38,** 308–321.

Veronis, G., 1966: Wind-driven ocean circulation—Part 2. Numerical solutions of the non-linear problem. *Deep-Sea Res.*, **13,** 31–55.

Worthington, L. V., 1976: *On the North Atlantic Circulation.* The Johns Hopkins University Press, 110 pp.